isvr Institute of Sound and Vibration Research

Active Vibration Isolation of a 3-Dimensional Structure using Velocity Feedback Control

S.M. Kim, S.J. Elliott and M. J. Brennan

ISVR Technical Memorandum 845

October 1999

University of Southampton

SCIENTIFIC PUBLICATIONS BY THE ISVR

Technical Reports are published to promote timely dissemination of research results by ISVR personnel. This medium permits more detailed presentation than is usually acceptable for scientific journals. Responsibility for both the content and any opinions expressed rests entirely with the author(s).

Technical Memoranda are produced to enable the early or preliminary release of information by ISVR personnel where such release is deemed to the appropriate. Information contained in these memoranda may be incomplete, or form part of a continuing programme; this should be borne in mind when using or quoting from these documents.

Contract Reports are produced to record the results of scientific work carried out for sponsors, under contract. The ISVR treats these reports as confidential to sponsors and does not make them available for general circulation. Individual sponsors may, however, authorize subsequent release of the material.

UNIVERSITY OF SOUTHAMPTON

INSTITUTE OF SOUND AND VIBRATION RESEARCH

SIGNAL PROCESSING & CONTROL GROUP

Active Vibration Isolation of a 3-Dimensional Structure using Velocity Feedback Control

by

S.M. Kim, S.J. Elliott and M.J. Brennan

ISVR Technical Memorandum No. 845

October 1999

Authorised for issue by
Prof S J Elliott
Group Chairman

Contents

Abstract

This report investigates the physical aspects and control mechanisms associated with an active vibration isolation system in which electromagnetic control actuators are installed in parallel with each of four mounts between a piece of equipment and a vibrating base structure. The control strategy used is *decentralised velocity feedback control*, where each of the four actuators is operated *independently* by feeding back the equipment absolute velocity response at the same location. The special feature of the model is that, although one ends of the actuators are collocated with the sensor locations, the control system is not collocation control because of the supporting force of each actuator acting on the flexible base structure whose dynamics are strongly coupled with the mounted equipment. In particular, isolation of low frequency vibration is considered where the equipment can be modelled as a being rigid and the mounts as lumped parameter springs and dampers. The impedance method is employed for the mechanical analysis of both passive and active vibration isolation systems. It is shown analytically that the system is unconditionally stable, and so perfect vibration isolation is theoretically achievable. The results from an experimental four-mount active isolation system are also discussed. The measured system response and closed loop attenuation is very similar to the predicted results, and up to 14 dB reduction in the kinetic energy of the equipment can be achieved in practice. If very high gains are used in the experiments, however, instability is encountered at about 1 Hz due to some undesirable phase shifts in the electrical equipment used.

1. Introduction

Vibration mounts (also called isolators) are generally required to protect a piece of delicate equipment in a severe vibration environment. Passive mounts, which may be modelled as both resilient and energy dissipating elements, are widely used to support the equipment and isolate it from base vibration. However, passive mounts have an inherent trade-off between low and high frequency isolation performances depending on the dissipating elements used [1]. Low mount damping brings poor performance at low frequencies, while high mount damping brings poor performance at high frequencies. Thus, for a further improvement of the isolation performance it is often required to introduce extra power sources that can actively reduce vibration transmission through the mounts at all frequencies. Active vibration isolation has been of great interest in various engineering fields, and many efforts have been made as reviewed in [2,3].

Although such an active isolator can be constructed by feeding back the full state variables, as commonly seen in work on active suspension [4,5], a more practical way may be direct output feedback control. The absolute velocity responses of a plant structure measured by sensors are often used as the feedback quantity. In particular, when the actuators are collocated with the sensors, then the multichannel control system is proven to be asymptotically stable[6,7]. In this case, the electric control gain used can be analogously transformed to a virtual mechanical skyhook damper [8]. Using the idea of the skyhook damper, Serrand[9] has presented an experimental study on a two-mount active isolation system to reduce vibration transmission into a two-dimensional symmetric rigid equipment structure which is installed statically balanced by two passive mounts on an excited flexible base structure. He has shown experimentally that the decentralised control configuration using the same gain in each control loop is capable to reduce equipment vibration at all frequencies of interest.

The work presented here is an extension to a more general four-mount active vibration isolation system for a three-dimensional equipment structure. There is, however, particular emphasis on the physical aspects and mechanisms of control including stability issues. Electromagnetic actuators are used as the control actuators of the active vibration isolation

system for convenience, and are installed between a piece of equipment and a flexible base structure in parallel with each of four mounts. The control strategy used is *decentralised velocity feedback control*[10,11], where each of the four actuators is operated *independently* by feeding back the equipment absolute velocity response at the same location. In particular, isolation of low frequency vibration is considered where the equipment can be considered to be being rigid and the mounts to be springs and dampers. The particular feature of this control configuration is that, although one ends of the actuators are collocated with the sensors, the control system is not collocation control. This is because the actuators are installed between the equipment and base structure for the convenience of practical implementation, and thus the actuators excite the base structure as well as the equipment. Because of this, when the flexible base structure is strongly coupled with the mounted equipment, the established theory for collocation control [6,7] is not directly applicable. The objective of this research was to clarify the performance and stability issues associated with this four-mount vibration isolation system using decentralised velocity feedback control. The basic concepts and mechanisms of velocity feedback control associated with this actuator installation are analysed in Section 2 first with a single-mount vibration isolation system. The impedance method, which is known a powerful tool in the analysis of coupled systems[12,13], is employed for the mechanical analysis of both passive and active vibration isolation systems. A proof of unconditional stability is given in Section 3 using the Nyquist criterion. The maximum allowable gain is also analytically addressed for a control system having a time delay in the control loop. The impedance method is extended to analyse a multiple-mount system including the four-mount system in Section 4, where both performance and stability issues are discussed. Some experiment results are presented and compared with simulation results in Section 5. Potential causes of instability in practical implementation are also addressed. Finally some conclusions are given in Section 6. There are also two appendices that give the relevant equations for the model problem used in the simulations and the experimental work.

2. Active vibration isolation of a single mount system

2.1 Analysis of the mounted equipment

Before dealing with a complex multiple-mount system, it is instructive to start with active vibration isolation in a single mount system where an equipment structure is supported upon a single mount. A simplified model is shown in Figure 1 where a rigid equipment of mass m_e is supported by a passive mount consisting of spring k_m and damper c_m. An electromagnetic control actuator generating the control force f_c is also installed between the equipment and base structure in parallel with the passive mount to achieve a further reduction of vibration transmission from the base velocity v_b to the equipment velocity v_e. The control system employs direct feedback control that uses the measured signal from the equipment v_e to operate the control force f_c via the controller which has gain $-H$. It is assumed that the mount is massless, and there is no time delay in the electric controller. The structure comprising the rigid equipment and the mount is referred as the mounted equipment.

Let the total force acting through the mount be f_m, then the mounted equipment can be described as

$$Z_e v_e = f_m \tag{1}$$

$$f_m = f_c + Z_i(v_b - v_e) \tag{2}$$

where $Z_e = j\omega m_e$ and $Z_m = c_m + k_m / j\omega$, and frequency dependency of all the variables are assumed since impedance is generally defined in the frequency domain. Transmissibility through the passive mount in the absence of the control force f_c is given by

$$T = \frac{v_e}{v_b} = \frac{Z_m}{Z_e + Z_m} \tag{3}$$

When direct feedback control is applied, the transmission ratio can be rewritten as

$$T_c = \frac{v_e}{v_b} = \frac{Z_m}{Z_e + Z_m + Z_c} \tag{4}$$

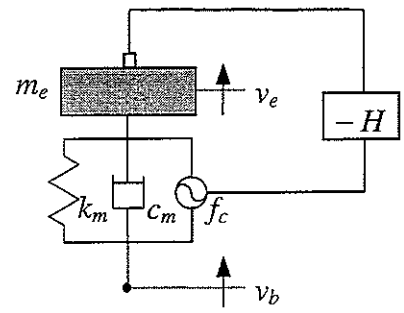

Figure 1. A simplified model of velocity feedback control

where Z_c is $H_d/j\omega$, H_u, or $j\omega H_a$ for displacement, velocity, or acceleration feedback, respectively. As far as the dynamic behaviour of the mounted equipment is concerned, the impedance Z_c due to control action can be exactly replaced by a passive mechanical element, provided the base input v_b is bounded regardless of the control action. Using equation (4), the control force f_c for each case can be written as

$$f_c = -Z_c v_e = -Z_c T_c v_b \tag{5}$$

When the gain for each control case is infinitely large, then $|Z_c| >> |Z_e + Z_m|$ in equation (4) so that the transmission ratio is greatly improved i.e. $T_c \approx 0$. For such a feedback gain, the control force f_c becomes

$$f_{co} \approx -Z_m v_b \tag{6}$$

The result shows that the control force when the feedback gain is infinite is the same as the *perfect control force* for a feedforward controller using the base response as the reference signal. More importantly, it suggests that perfect control can be *approximately* achieved when the direct output feedback control technique is applied with an infinite gain, regardless of whether displacement, velocity, or acceleration feedback is used. Feedback control is generally preferable for practical implementation, since it is easier to implement and is more robust to plant uncertainty than feedforward control[14]. From substituting equations (2) and (6) into (1), when the base velocity v_b is bounded, it can be seen that the equipment is stable to base excitation as well as any possible external force excitation on the equipment. However, when $f_c = Z_m(v_e - v_b)$, the equipment would be motionless but unstable to disturbances because no spring and damper elements exist.

To compare control performances for each response control case, Figure 2 shows transmissibility for a single d.o.f mounted equipment of mass $m_e = 1$ kg, natural frequency $f_n = 20$ Hz and damping ratio $\varsigma = 0.05$. Feedback gains used are $H_d = Hk_m$, $H_v = Hc_m$ and $H_a = Hm_e$ where H = 10. It clearly demonstrates that there is an advantageous frequency region for each feedback control: displacement, velocity and acceleration feedback control techniques are effective for stiffness, damping and mass governed frequency regions, respectively. As discussed above, the effective control regions are where $|Z_c| >> |Z_e + Z_m|$. Velocity feedback control acts as an added damper (so-called skyhook damper[8]) and reduces the response at resonance. Added effective stiffness and inertia to the equipment through feedback control change the natural frequencies of the displacement and acceleration feedback control systems, respectively. The control forces for each case were also calculated using equation (5), and are compared in Figure 3 with the perfect control force calculated from equation (6). In the effective region of each controller, the control forces are close to the perfect control force. As the gain H for each controller increases, a better control performance and a closer resemblance of the perfect force is achieved. Unlike the cases for displacement and acceleration feedback control, control force for velocity feedback control approaches the perfect control force without having a peak at low or high frequencies. Moreover, velocity feedback control is known to be a more robust control strategy than the others, as far as unmodelled phase shifts are concerned [3,7]. Thus, hereafter in this report velocity feedback is the only control technique considered.

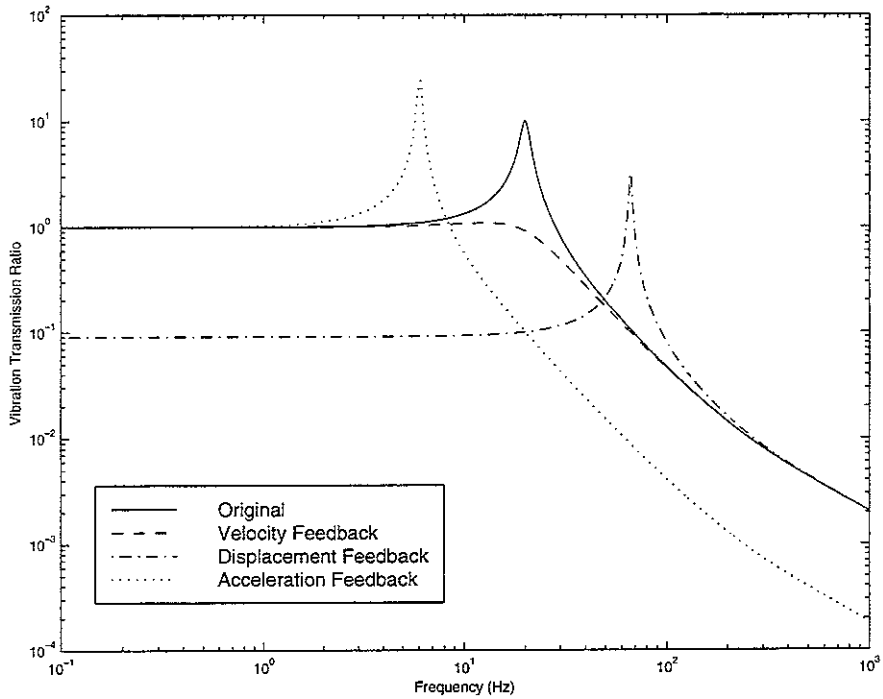

Figure 2. Control performances of displacement, velocity and acceleration feedback.

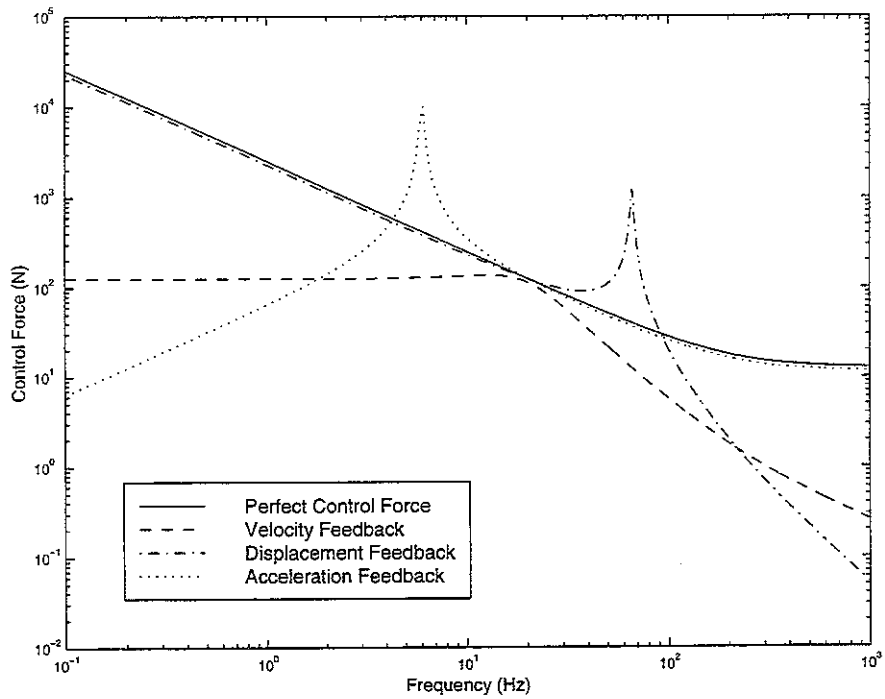

Figure 3. Control forces for displacement, velocity and acceleration feedback compared with the optimal force

2.2 Analysis of the complete coupled system

In this section the analysis of the single mount system is continued but with consideration of the dynamics of the flexible base structure that is strongly coupled with the mounted equipment. The complete coupled system connected by a single mount can be represented in terms of impedances as shown in Figure 4(a), where Z_e, Z_m, and Z_b denote the impedances of the equipment, mount, and base, respectively. The base structure is excited by a primary force f_p, and a pair of control forces f_c located in parallel with the mount act on both the equipment and the base structure. The control forces can model an electromagnetic actuator installed between the equipment and base structure. As a simple illustration of the single mount system, Figure 4(b) shows a two d.o.f system where a rigid piece of equipment with impedance $Z_e = j\omega m_e$ is installed on a single degree-of-freedom vibrating base structure with impedance $Z_b = j\omega m_b + c_b + k_b/j\omega$ through a mount consisting of a spring and damper $Z_m = c_m + k_m/j\omega$. It is convenient to interpret the whole system as a coupled one between the mounted equipment and the base structure, where the mounted equipment is the combination of the equipment and the mount. It is again assumed that the mount is massless. The complexity of this system stems from the fact that the force acts on both the equipment and the base structure. This is thus not collocation control in a usual sense[6,7], and subsequent mechanical and stability analyses need to be investigated.

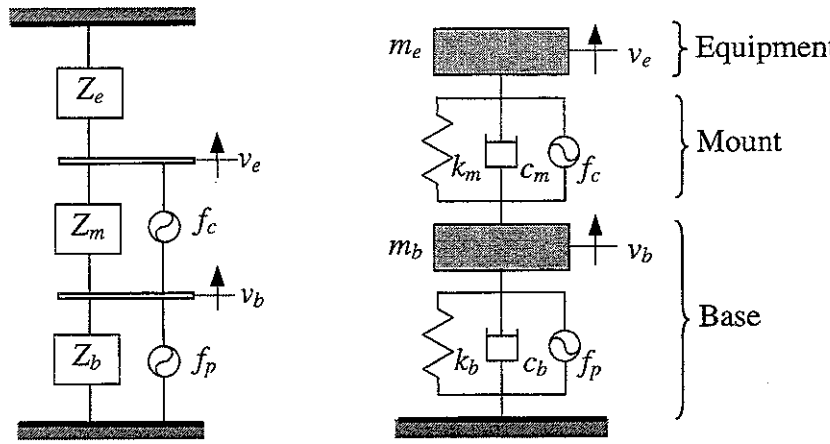

(a) Impedance representation (b) a two d.o.f system

Figure 4. A single mount vibration isolation system

Using the impedance approach, the base response can be written as

$$Z_b v_b = f_p - f_m \tag{7}$$

where f_m is the total force acting through the mount as given in equation (2). By combining equation (7) with the equations for the mounted equipment given in equations (1) and (2), the dynamic behaviour of the whole system can be described by the matrix equation

$$\begin{bmatrix} Z_e + Z_m & -Z_m \\ -Z_m & Z_b + Z_m \end{bmatrix} \begin{Bmatrix} v_e \\ v_b \end{Bmatrix} = \begin{Bmatrix} f_c \\ f_p - f_c \end{Bmatrix} \tag{8}$$

Because the passive system is stable, the velocity responses can be obtained by inverting the impedance matrix in equation (8). When velocity feedback control is applied with the control force $f_c = -Hu$, equation (8) becomes

$$\begin{bmatrix} Z_e + Z_m + H & -Z_m \\ -(Z_m + H) & Z_b + Z_m \end{bmatrix} \begin{Bmatrix} u \\ u_b \end{Bmatrix} = \begin{Bmatrix} 0 \\ f_p \end{Bmatrix} \tag{9}$$

Note that the whole system impedance matrix is now non-symmetric. It should be noted that, although one end of the actuator is collocated with the sensor on the equipment, the control system is not collocation control. This is because of the additional force acting on the base, and that makes the impedance matrix non-symmetric and the corresponding analysis non-trivial. Thus, the stability of the system can not be assessed by simply using the definiteness property (positive or negative) of the impedance matrix as in collocation control[6,7]. In addition, an understanding using the mechanical analogy such as a skyhook damper[8] is no longer correct, as far as the dynamics of the complete coupled system is concerned. Stability is rigorously analysed in Section 3, and so it is initially assumed to be stable in this section.

Equation (9) can be simplified when the base structure is weakly coupled with the mounted equipment system. Since the reaction force from the mount is then negligible compared with the primary force i.e., $|f_m| << |f_p|$ in equation (7), equation (9) for *weak coupling* becomes

$$\begin{bmatrix} Z_e + Z_m + H & -Z_m \\ 0 & Z_b \end{bmatrix} \begin{Bmatrix} u \\ u_b \end{Bmatrix} = \begin{Bmatrix} 0 \\ f_p \end{Bmatrix} \tag{10}$$

It can be seen that the base behaves as if there were no mounted equipment attached, and its resulting response acts as the excitation input to the mounted equipment. A detailed discussion on weak coupling can be found in [13].

If the perfect control force is applied i.e. $f_{co} = -Z_m v_b$ in equation (6), equation (9) becomes

$$v_e \approx 0, \qquad v_b \approx Z_b f_p \tag{11}$$

This result states that, when the gain is infinitely large, the perfect control force *uncouples* the mounted equipment from the base. In this case, perfect control of equipment vibration can be achieved, and the base behaves as if no mounted equipment were attached.

In the previous section, control performance was discussed in term of transmissibility $T_c = v_e / v_b$ without regard to the dynamics of the base. It is a good performance measure for a weakly coupled mounted equipment-base system where the denominator v_b of T_c is an independent input to the system so that it remains the same before and after the installation of the mounted equipment. In a strongly coupled system as represented in equation (8), however, v_b changes after attachment as well as a change of control gain so that transmissibility T_c does not represent the absolute vibration response of the equipment v_e. Thus the absolute velocity of the equipment is more preferable as a performance measure in this case, and for a multiple d.o.f equipment the kinetic energy of the equipment may be a good performance measure. To support this, some simulations were conducted for the two d.o.f system shown in Figure 4(b). The upper single d.o.f mounted equipment system was assumed to be of mass $m_e = 1\,kg$, natural frequency $f_n = 20\,Hz$ and damping ratio $\varsigma = 0.05$, and the lower single d.o.f base system was assumed to be of mass $m_b = 1\,kg$, natural frequency $f_n = 30\,Hz$ and damping ratio $\varsigma = 0.01$. The physical parameters used are the same as those used for Figure 2. It is known that, when the uncoupled natural frequencies are close, they are generally strongly coupled so that the fully coupled model given in equation (9) should be used. The dynamics of the two d.o.f system are well known [15], and may be sufficient to investigate basic coupling mechanisms during active control.

The results are shown in Figure 5 both before and after control cases. Due to strong coupling, the natural frequencies of the coupled system are different from the uncoupled natural frequencies. In addition, there is a sharp anti-resonance at the uncoupled natural frequency of the mounted equipment in Figure 5(b) since the mounted equipment acts as a dynamic neutraliser at the frequency [16]. Referring to Figure 5(a), the maximum velocity reduction after control is not at the natural frequency of the uncoupled mounted

equipment, but at the natural frequencies of the whole coupled system. Figure 5(a, b) clearly demonstrate that the high reduction of the vibration transmission ratio at the natural frequency of the uncoupled mounted equipment in Figure 2 is due to the increased base velocity after control. The results clearly demonstrate that the controller *uncouples* the isolator from the base as the gain increases.

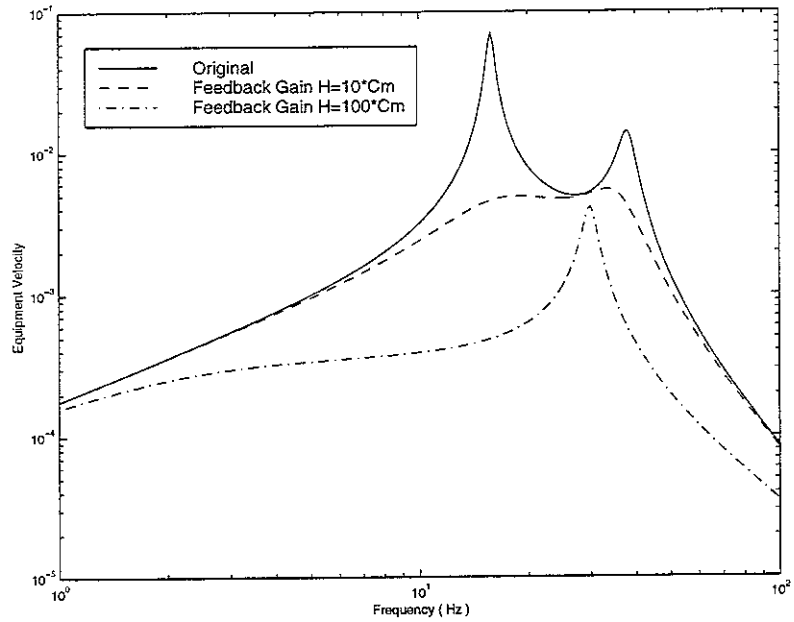

(a) Equipment velocity

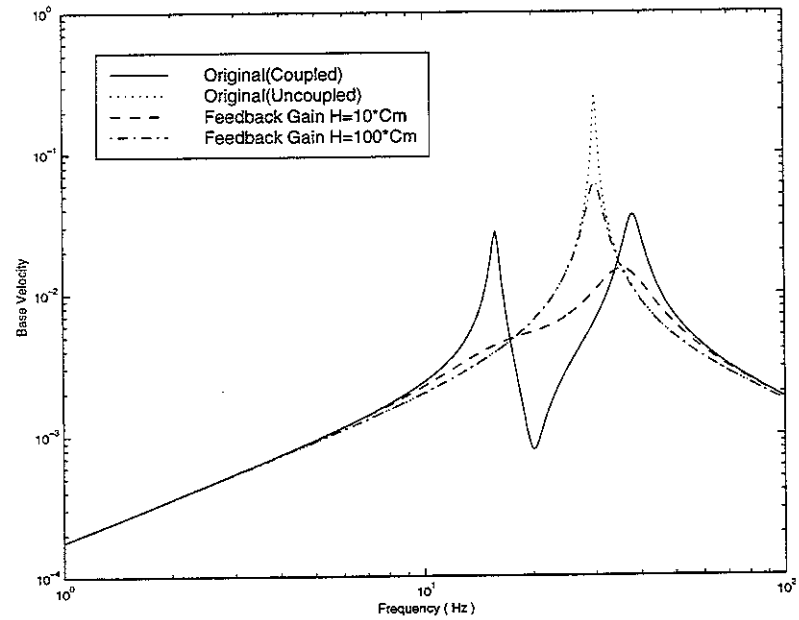

(b) Base velocity

Figure 5. Dynamics of a simple 2 dof system; before control (solid line), after control (dashed line)

3. Stability analysis of the single mount system

3.1 Unconditional stability

This section considers stability analysis of the single mount system shown in Figure 4. The control system can be represented for the equipment response v_e by using a block diagram for disturbance rejection problems as shown in Figure 6. By inverting the impedance matrix in equation (8), we can express the equipment velocity as

$$v_e = G(j\omega) f_c + d_e \tag{12}$$

where the frequency response of the plant $G(j\omega)$ is given by

$$G(j\omega) = \frac{v_e}{f_c} = \frac{1}{Z_e + Z_m + Z_m Y_b Z_e} \tag{13}$$

and the disturbance is $d_e = Y_b Z_m f_p / (Z_e + Z_m + Z_m Y_b Z_e)$ in which the driving point mobility of the base is $Y_b = 1/Z_b$. If feedback control is applied so that $f_c = -Hv_e$, then the equipment velocity is

$$v_e = \frac{d_e}{1 + G(j\omega)H} \tag{14}$$

Similarly, the base velocity after feedback can be obtained as

$$v_b = \frac{Z_e + Z_m + H}{1 + G(j\omega)H} \cdot \frac{d_e}{Z_m} \tag{15}$$

Using the Nyquist stability criterion, the responses in equations (14) and (15) are *stable* i.e. internally stable[11], if and only if the common open loop frequency response function $L(j\omega) = G(j\omega)H$ does not enclose the $(-1, 0)$ point in the complex $L(j\omega)$ plane. Since H is a positive gain, the control system is *unconditionally stable* if and only if the plant $G(j\omega)$ does not cross the negative real axis.

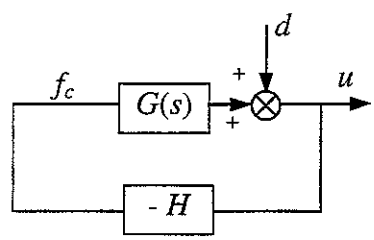

Figure 6. General block diagram representation of disturbance rejection.

Unconditional stability is examined first for the case when the mounted equipment is weakly coupled with the base structure, and then is extended to strongly coupled cases. The degree of coupling can be judged by comparing dynamic characteristics of the uncoupled systems at the connection point v_b, and is given by [12,13]

$$\left|Z_{me}Y_b\right| << 1 \tag{16}$$

where the input impedance to the mounted equipment is $Z_{me} = Z_m Z_e/(Z_m + Z_e)$. Applying equation (16) to (13) the weakly coupled plant can be written as

$$G(j\omega) = \frac{1}{Z_e + Z_m} \tag{17}$$

It is important to note that $\mathrm{Re}(Z) \geq 0$, where $Z = Z_e + Z_m$ and Re(•) denotes the real part. Thus the plant has the characteristic of

$$\mathrm{Re}(G(j\omega)) \geq 0 \qquad \text{or} \qquad 90° \leq \angle G(j\omega) \leq 90° \tag{18}$$

The plant Nyquist locus resides on the right half of the complex plane, and thus it never crosses the negative real axis. Thus the control system for the weakly coupled plant is unconditionally stable. Equation (18) is a necessary condition for the plant to be the driving point mobility of a passive system. In fact, equation (17) is the driving point mobility of the mounted equipment installed on a rigid base. When the mounted equipment is weakly coupled with the base, therefore the plant turns into the driving point mobility, and is unconditionally stable.

However, when the mounted equipment and the base structure are strongly coupled, the stability analysis is more complicated because the force acting on the base now affects the dynamic response of the equipment. The real part of the plant given in equation (13) is determined by the third term in the denominator $Z_m Z_e Y_b$ because of the non-negative definite property $\mathrm{Re}(Z_e) \geq 0$ and $\mathrm{Re}(Z_m) \geq 0$. Let the equipment of a typical single d.o.f system be installed on a flexible structure as shown in Figure 7(a). The impedances of this system are given by $Z_m = k_m / j\omega$ and $Z_e = j\omega m_e \omega_e^2 / (\omega_e^2 - \omega^2)$ where ω_e is equal to $\sqrt{k_e/m_e}$ which corresponds to the angular natural frequency of the first flexible mode of the equipment. For simplicity, damping in the equipment and the mount is ignored.

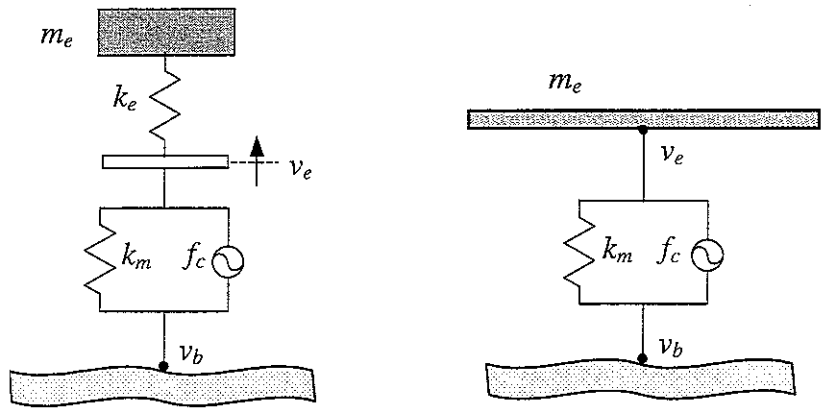

Figure 7. Rigid(a) and flexible(b) equipment structures mounted on a flexible structure

Applying the condition in equation (18) to this term gives

$$m_e k_m \left(\left(\omega_e^2 - \omega^2 \right) / \omega_e^2 \right) \cdot \mathrm{Re}(Y_b) \geq 0 \tag{19}$$

Since the real part of the base mobility Y_b is always non-negative, equation (19) is valid at the low frequency range where $\omega < \omega_e$. When the equipment has only an inertial element i.e. $Z_e = j\omega m_e$, equation (19) becomes $m_e k_m \cdot \mathrm{Re}(Y_b) \geq 0$ so that equation (18) is satisfied at all frequencies. The Nyquist locus for the inertial equipment is always on the right half complex plane. If a small damping in the mount is included, the original locus is slightly declined to the clockwise direction, but approaches to the origin as the frequency increases without crossing the negative real axis. An important conclusion from this analysis is that the system is unconditionally stable regardless of the degree of coupling, *if and only if* the equipment is rigid and is supported only upon a massless mount.

As a general example of the equipment, consider a free-free beam installed on a flexible base through a single mount as shown in Figure 7(b). As is shown in Appendices A and B, the driving point mobility of the beam can be represented as a summation of N modes. When the beam of mass m_e is mounted at its mid-point $L/2$, the driving point mobility is given by

$$Y_e = \frac{1}{j\omega m_e} + \frac{1}{m_e} \sum_{n=3}^{N} \phi_n^2 (L/2) A_n(\omega) \tag{20}$$

where the first term denotes the rigid body mode and the second term denotes higher flexible modes. Since the driving point is at the mass centre, the rigid body mode corresponding to $n=2$ is not excited. In addition, ϕ_n is the *n-th* mode shape, and the vibration modal resonance term $A_n(\omega)$ is $A_n(\omega) = j\omega/\left(\omega_n^2 - \omega^2 + j2\zeta_n\omega_n\omega\right)$ in which ω_n and ζ_n are the natural frequency and the damping ratio of *n-th* mode, respectively. If again no damping is assumed in the equipment and the mount, the real part of the plant in equation (13) is governed by the real part of $Z_m Y_b Z_e$. Only the first two modes of the beam that are excited are considered for simplicity. An unconditional stability condition corresponding to equation (19) can be written as

$$\mathrm{Re}\left(m_e k_m \frac{\omega_e^2 - \omega^2}{\omega_e^2 - \omega^2(1+\phi^2)} Y_b \right) \geq 0 \tag{21}$$

where $\omega_e = \omega_n$ and $\phi^2 = \phi_n^2(L/2)$ for the first excited flexible mode. Since Y_b is a driving point mobility and $\phi^2 \geq 0$, the condition in equation (21) is satisfied, provided that

$$\omega \leq \sqrt{\frac{\omega_e^2}{1+\phi^2}} \tag{22}$$

The result shows that, if there is a flexible mode in the equipment structure that is strongly coupled with the flexible base, the system may become unstable at high frequencies. Such a potential instability problem at high frequencies may be avoided by low-pass filtering of the measured sensor signal in practice. Nevertheless it is clear that, at frequencies far lower than the first exciting flexible equipment mode, the plant is unconditionally stable. Thus, *if and only if* the equipment is rigid and is supported only upon a massless mount, the active isolation system shown in Figure 4 has *collocation control-like* behaviour(unconditionally stable and perfect controllability) and its plant shows *driving point mobility-like* behaviour(no crossover the negative real axis of the Nyquist plot).

3.2 The effect of a time delay

The stability analysis considered in the previous section was for an idealised model assuming perfect modelling of the mechanical and electrical systems together with no time delay on the control loop. An infinitely large gain in this case can result in perfect vibration isolation. However, such an idealised condition is rarely met in practice, and an increasing gain eventually causes instability. In particular, time delays in the open loop

frequency response function $L(j\omega)$ would be one of most crucial factors. The origins of such a time delay are various, for example, use of lowpass filters for sensing, phase lags in actuators and power amplifiers, etc. Time delays should be avoided as much as possible for a better performance. This section considers the theoretical analysis of stability for an active isolation system with a pure time delay in $L(j\omega)$. In practice, physical systems are quite complicated and modelling errors would not be exactly represented by a pure time delay. However it should be emphasised that analytical studies considered in this report would facilitate insight into the limitations of collocation-like control. Stability analysis for the weakly coupled equipment-base system is first considered, and is extended to the fully coupled case.

When the equipment-base system is weakly coupled and there is a pure time delay in the controller, the open loop frequency response function $L(j\omega)$ can be rewritten as

$$L(j\omega) = \frac{He^{-j\omega\tau}}{Z_e + Z_m}, \tag{23}$$

where the weakly coupled plant $G(j\omega) = 1/(Z_e + Z_m)$, H is the proportional control gain, and $e^{-j\omega\tau}$ is the frequency domain representation of the pure time delay τ in the controller. The maximum value of the control gain H depends on the time delay τ, and its relationship can be calculated by the Nyquist stability criterion [14]. For a given gain margin (GM), equation (23) for the single d.o.f mounted equipment in Figure 4(b) can be written as

$$L(j\omega_c) = \frac{j\omega_p H_{max} e^{-j\omega_p\tau}}{k_m - m_e\omega_p^2 + j\omega_p c_m} = -\frac{1}{GM} \tag{24}$$

where H_{max} is the maximum allowable gain for the gain margin denoted as GM on the right side, ω_p is the phase crossover frequency at which the phase is -180°. If the time delay is very small compared with the natural period of the mounted equipment so that $\omega_p >> \omega_n$, where the angular natural frequency of the mounted equipment is $\omega_n = \sqrt{k_m/m_e}$, an approximate solutions of equation (24) can be obtained. They are given by[14]

$$\omega_p \approx \frac{\pi}{2\tau}, \qquad H_{max} \approx \frac{m_e\omega_p}{GM} \tag{25,26}$$

It can be seen that as the delay τ increases, the phase crossover frequency ω_p in equation (25) decreases so that the maximum allowable gain H_{max} gets smaller in equation (26).

When the mounted equipment is strongly coupled with the base, the plant $G(j\omega)$ includes the mobility of the base Y_b as given in equation (13). However, it is not necessary to consider the fully coupled model to obtain the crossover frequency ω_c and the maximum allowable gain H_{max}. This is because, when the time delay is very small compared with the natural periods of both the mounted equipment and the base so that $\omega_p >> \omega_n$, the dynamics of the coupled system near the phase crossover frequency ω_p is generally no longer strongly coupled. Thus the results in equations (25) and (26) are still valid for fully coupled systems.

Figure 8(a) shows the Nyquist plot for the system considered in Section 2 but with a time delay of 0.5 ms together with the assumption of weak coupling. The maximum allowable gain H_{max} was calculated from equation (26) for the gain margin $GM = 2$. The Nyquist plot passes approximately $(-1/2, 0)$ at about the phase crossover frequency 500 Hz obtained from equation (25). When the feedback gain is increased more than twice of H_{max}, the control system encircles the Nyquist point (-1, 0) in the plot and thus becomes unstable. The Nyquist plot for the fully coupled model is shown in Figure 8(b) with using the same H_{max}. It can be seen that near and over the crossover frequency ω_c there is no discernible difference between Figure 8(a) and Figure 8(b). The open loop frequency response functions for both weak and full coupling models are also shown together in Figure 9 as Bode plot form for clarity. Figure 10 shows the transmissibility graphs for the models with and without the pure time delay. The system with the time delay shows the 'waterbed effect' around the crossover frequency[10].

Overall, concepts and mechanisms of active isolation have been discussed for a single mount system. It has been shown that collocation control of rigid equipment responses with an infinite gain is the same as perfect feedforward control using the base velocity reference input in terms of performance. The mechanism involved with the active isolation system considered is that, as the gain increases, the controller uncouples the mounted equipment from the base. The kinetic energy of the equipment is suggested as the measure of control performance. Unconditional stability has been proven for a rigid equipment mounted on a massless mount. In addition, stability for a control system with a pure time delay on its control loop has been examined. In the following section, the impedance

approach for a single mount system represented in equation (9) is extended to the case of a multiple-mount system.

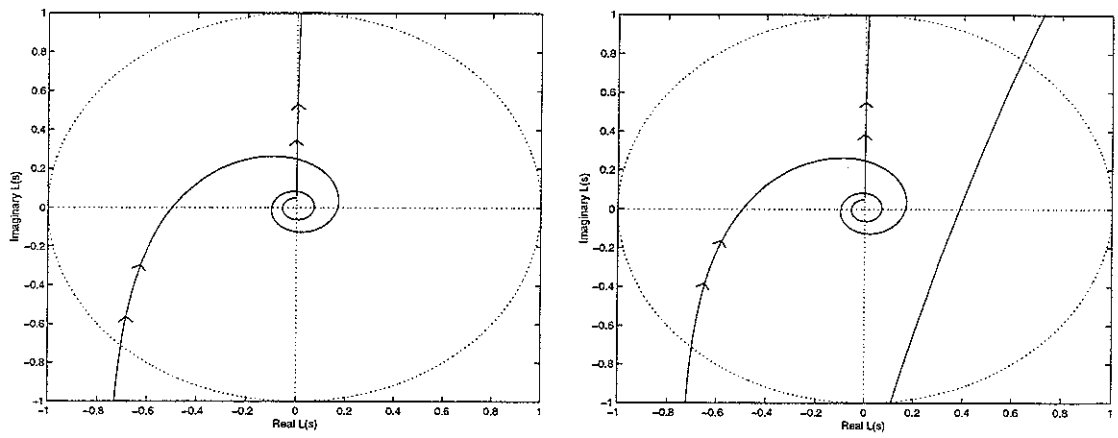

(a) Weakly coupled model (b) Fully coupled model

Figure 8. Nyquist plot for weakly and fully coupled models

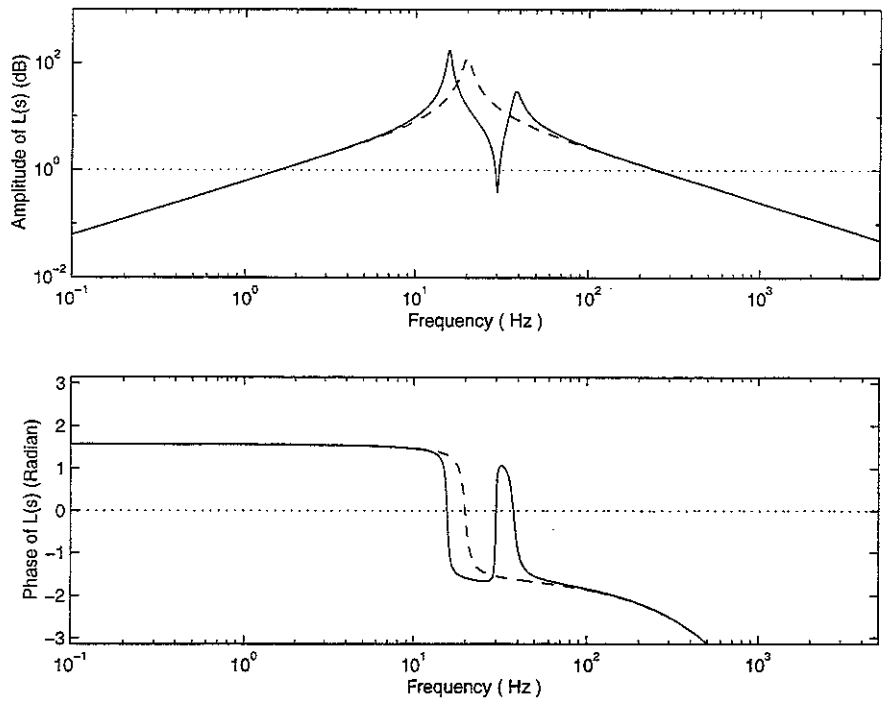

Figure 9. Bode plots for weakly(dashed) and fully(solid) coupled models

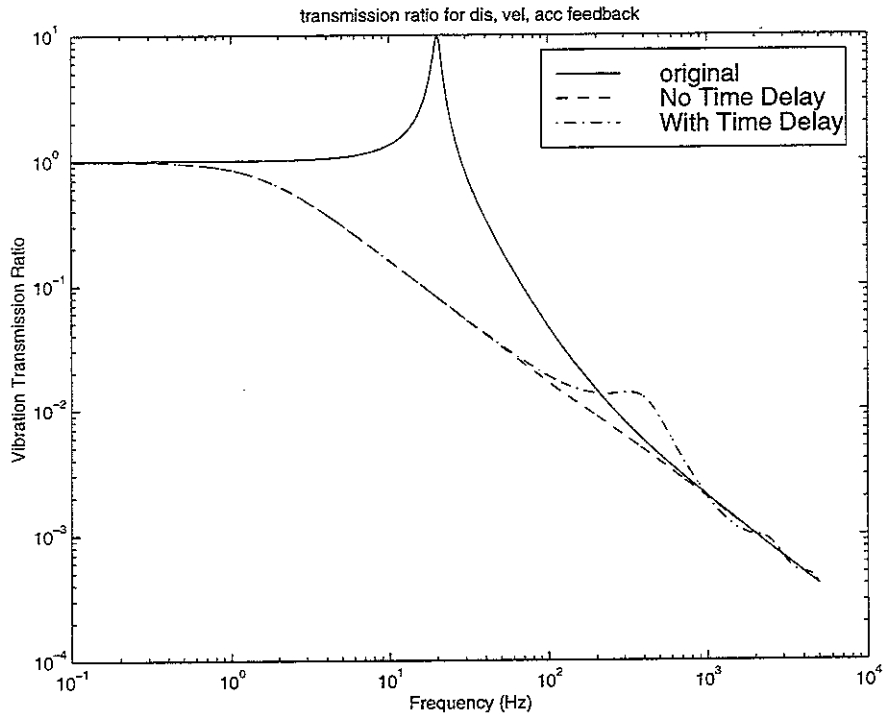

Figure 10. Velocity transmission ratios for with and without considering the pure time delay

4. Active vibration isolation of a multiple-mount system

4.1 Flexible equipment

This section considers a generalisation of the impedance representation described in Section 2 to cover the general case where a flexible equipment structure is connected to a base structure through a set of multiple mounts. The multiple mount vibration isolation system can be represented by an impedance diagram as shown in Figure 11, which is a simple extension of Figure 4(a). The vector $\mathbf{d_p}$ is introduced because $\mathbf{f_p}$ is not collocated with $\mathbf{f_c}$. The number of mounts is M, and the total number of modes in the flexible equipment and base structures are N and L, respectively. Again no mass effects are considered in the mounts. Since M mounts are used, the end velocities of all mounts are denoted as M length vectors $\mathbf{v_e}$ to the equipment and $\mathbf{v_b}$ to the base, respectively. The equipment subject to multiple mount forces $\mathbf{f_m}$ can be written as

$$\mathbf{Z}_e \mathbf{v}_e = \mathbf{f}_m, \tag{27}$$

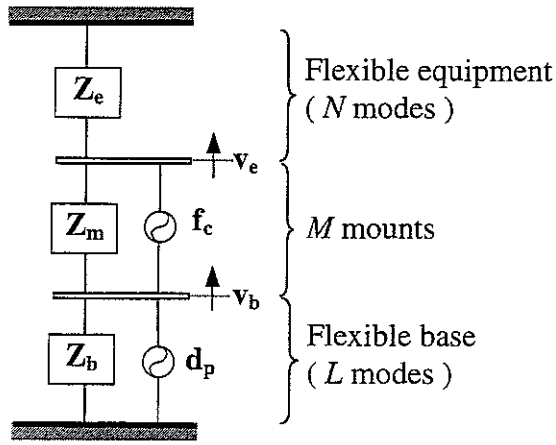

Figure 11. A multiple mount vibration isolation system

where $\mathbf{Z}_e = \mathbf{Y}_e^{-1}$, provided the input mobility matrix $\mathbf{Y}_e$ is invertible. The mobility matrix is invertible if the elements of the vector $\mathbf{v}_e$ are linearly independent. By extending equation (2) for a single mount, the mount force vector can be written as

$$\mathbf{f}_m = \mathbf{f}_c + \mathbf{Z}_m(\mathbf{v}_b - \mathbf{v}_e), \tag{28}$$

where the impedance matrix of the mounts $\mathbf{Z}_m$ is a ($M \times M$) diagonal matrix whose diagonal terms are the impedances of each mount. Again by extending equation (7), the base response can be written as

$$\mathbf{Z}_b \mathbf{v}_b = \mathbf{d}_p - \mathbf{f}_m, \tag{29}$$

where $\mathbf{d}_p = \mathbf{Z}_b \mathbf{Y}_{bp} \mathbf{f}_p$ in which $\mathbf{Y}_{bp}$ are the mobility matrix of the uncoupled base due to the primary force vector $\mathbf{f}_p$. The impedance of the uncoupled base due to the mount force vector $\mathbf{f}_m$ is $\mathbf{Z}_b = \mathbf{Y}_b^{-1}$, provided $\mathbf{Y}_b$ is invertible. Combining equations (27-29) gives

$$\begin{bmatrix} \mathbf{Z}_e + \mathbf{Z}_m & -\mathbf{Z}_m \\ -\mathbf{Z}_m & \mathbf{Z}_b + \mathbf{Z}_m \end{bmatrix} \begin{Bmatrix} \mathbf{v}_e \\ \mathbf{v}_b \end{Bmatrix} = \begin{Bmatrix} \mathbf{f}_c \\ \mathbf{d}_p - \mathbf{f}_c \end{Bmatrix} \tag{30}$$

This is a compact description of the mounted equipment-base coupled system in terms of impedances at the mount locations. Note this is also a simple extension of the single mount system in equation (8). Note also that the conditions used for constructing the matrix equation are that $\mathbf{Y}_e$ and $\mathbf{Y}_b$ are invertible. If the total number of equipment modes N is not less than the number of mounts i.e. $N \geq M$, the matrix $\mathbf{Y}_e$ is generally invertible. The same applies to $\mathbf{Y}_b$ so that the condition is $L \geq M$ where L is the total number of base

modes considered. In this case, the responses in $\{\mathbf{v}_e \quad \mathbf{v}_b\}^T$ are linearly independent and the complete system impedance matrix of ($2M \times 2M$) size is invertible.

Applying velocity feedback control by setting $\mathbf{f}_c = -\mathbf{H}\mathbf{v}_e$, the system equation becomes

$$\begin{bmatrix} \mathbf{Z}_e + \mathbf{Z}_m + \mathbf{H} & -\mathbf{Z}_m \\ -(\mathbf{Z}_m + \mathbf{H}) & \mathbf{Z}_b + \mathbf{Z}_m \end{bmatrix} \begin{Bmatrix} \mathbf{v}_e \\ \mathbf{v}_b \end{Bmatrix} = \begin{Bmatrix} \mathbf{0} \\ \mathbf{d}_p \end{Bmatrix} \tag{31}$$

When $\mathbf{f}_c = -\mathbf{Z}_m \mathbf{v}_b$ in equation (28), the mounted equipment and the base are uncoupled so that perfect vibration isolation can be achieved. If the controlled system is stable, the velocities at both ends of the mounts can be obtained by taking the inverse of the total system impedance matrix.

As suggested earlier, the kinetic energy of the equipment can be used as the performance measure. However, in general the number of equipment modes is bigger than that of mounts i.e., $M < N$, and it is thus not possible to obtain the kinetic energy of the equipment from equation (31) which only gives velocity responses at the mount locations. Thus it is necessary to consider the dynamics of the equipment in modal co-ordinates. If one assumes that the equipment is a flexible plate described by the co-ordinate system $\mathbf{r}$, the kinetic energy is given by

$$E_k = \frac{\rho_e h}{2} \int_{S_e} |v_e(\mathbf{r}, \omega)|^2 dS \tag{32}$$

where, $v_e(\mathbf{r}, \omega)$ is the velocity at the position $\mathbf{r}$, and ρ_e, h, and S_e are the material density, thickness and area of the plate, respectively. When the vibration response in the flexible structure is assumed to be described by a summation of N modes, then the vibration velocity at position $\mathbf{r}$ can be written as [12]

$$v_e(\mathbf{r}, \omega) = \sum_{n=1}^{N} \psi_n(\mathbf{y}) a_n(\omega) = \boldsymbol{\psi}^T \mathbf{a} \tag{33}$$

where ^{T} denotes the transpose, and the N length column vectors $\boldsymbol{\psi}$ and $\mathbf{a}$ consist of the array of vibration mode shape functions $\psi_n(\mathbf{r})$ and the complex amplitude of the vibration velocity modes $a_n(\omega)$ respectively, where modes means those for the uncoupled plate, not for the complete coupled system. If the mode shape function denoted as $\psi_n(\mathbf{r})$ is normalised to be $S_e = \int_{S_e} \psi_n^2(\mathbf{r}) dS$, the kinetic energy given in equation (32) can be rewritten as

$$E_k = \frac{M_e}{2}\mathbf{a}^{\mathrm{H}}\mathbf{a} \tag{34}$$

where M_e is the total mass of the flexible plate i.e. $M_e = \rho_e h S_e$ and the superscript $^{\mathrm{H}}$ denotes the Hermitian transpose. In order to calculate the kinetic energy, equation (31) which is written in terms of the physical velocity response vector $\mathbf{u}$ should be represented in terms of the modal amplitude vector $\mathbf{a}$. By extending equation (33), the equipment velocity response vector $\mathbf{v}_e$ at the mount positions can be written as

$$\mathbf{v}_e = \Psi_M^{\mathrm{T}}\mathbf{a} \tag{35}$$

where the matrix Ψ_M^{T} is a transformation matrix which transforms the N length modal amplitude vector $\mathbf{a}$ to the M length physical velocity amplitude vector $\mathbf{v}_e$. Since Ψ_M^{T} is a (M×N) size matrix where $M < N$ (underdetermined), $\mathbf{a}$ can not be obtained from $\mathbf{v}_e$ [17]. It equivalently means that the inverse of Ψ_M^{T} does not exist even in the least square sense. This is the reason why one ought to use a modal domain formulation considered here. From Appendix A, the modal amplitude vector can be written analogously to equation (27) as follows:

$$\overline{\mathbf{Z}}_e\mathbf{a} = \mathbf{g}_m \tag{36}$$

where the equipment modal mobility matrix is $\overline{\mathbf{Z}}_e = \overline{\mathbf{Y}}_e^{-1}$, and $\mathbf{g}_m$ is the M length generalised force vector. The notation $\overline{\mathbf{Y}}_e$ is used for a mobility in modal co-ordinates to distinguish it from that in physical co-ordinates $\mathbf{Y}_e$. By multiplying the transformation matrix Ψ_M to both sides of equation (28), the generalised mount force vector is written as

$$\mathbf{g}_m = \Psi_M\mathbf{f}_c + \Psi_M\mathbf{Z}_m(\mathbf{v}_b - \mathbf{v}_e), \tag{37}$$

where $\mathbf{g}_m = \Psi_M\mathbf{f}_m$. A detailed description for the modal domain analysis is given in Appendix A. By combining equations (29), (36) and (37), the whole system matrix equation in modal co-ordinates is given by

$$\begin{bmatrix} \overline{\mathbf{Z}}_e + \overline{\mathbf{Z}}_m + \overline{\mathbf{H}} & -\Psi_M\mathbf{Z}_m \\ -(\mathbf{Z}_m + \mathbf{H})\Psi_M^{\mathrm{T}} & \mathbf{Z}_b + \mathbf{Z}_m \end{bmatrix} \begin{Bmatrix} \mathbf{a} \\ \mathbf{v}_b \end{Bmatrix} = \begin{Bmatrix} \mathbf{0} \\ \mathbf{d}_p \end{Bmatrix} \tag{38}$$

where the modal impedance matrices are given by

$$\overline{\mathbf{Z}}_m = \Psi_M\mathbf{Z}_m\Psi_M^{\mathrm{T}} \qquad \overline{\mathbf{H}} = \Psi_M\mathbf{H}\Psi_M^{\mathrm{T}} \qquad \overline{\mathbf{Z}}_e = \overline{\mathbf{Y}}_e^{-1} \tag{39a,b,c}$$

Note that $\overline{\mathbf{Z}}_m$ and $\overline{\mathbf{H}}$ are obtained by transformations from physical co-ordinates into the equipment modal co-ordinates, while $\overline{\mathbf{Z}}_e$ is directly obtained from the inverse of $\overline{\mathbf{Y}}_e$. Note

the matrix $\overline{\mathbf{Z}}_e$ of rank N can not be obtained from $\Psi_M \mathbf{Z}_e \Psi_M^T$ whose rank is M, where $N > M$. Note also $\overline{\mathbf{Z}}_e$ is diagonal, while $\overline{\mathbf{Z}}_m$ is generally non-diagonal but symmetric although $\mathbf{Z}_m$ is diagonal. The non-diagonal terms act as coupling terms between equipment modal responses. The general representation in equation (38) is valid regardless of the difference of M and N. The modal amplitude vector **a** obtained from equation (38) is substituted into equation (34) to calculate the equipment kinetic energy. It can also be substituted to equation (35) to obtain the physical velocity vector $\mathbf{v}_e$.

Consider when $M = N$ and $M < L$, where L is the number of base modes considered. In this case, the transformation matrix Ψ_M^T in equation (35) is now square (fully determined). If it is assumed to be invertible, equation (38) can be further simplified as

$$\begin{bmatrix} \overline{\mathbf{Z}}_e + \overline{\mathbf{Z}}_m + \overline{\mathbf{H}} & -\overline{\mathbf{Z}}_m \\ -(\overline{\mathbf{Z}}_m + \overline{\mathbf{H}}) & \overline{\mathbf{Z}}_b + \overline{\mathbf{Z}}_m \end{bmatrix} \begin{Bmatrix} \mathbf{a} \\ \mathbf{b} \end{Bmatrix} = \begin{Bmatrix} \mathbf{0} \\ \Psi_m \mathbf{d}_p \end{Bmatrix} \tag{40}$$

where the modal amplitude vectors are given by

$$\mathbf{a} = \left(\Psi_M^T\right)^{-1} \mathbf{v}_e, \qquad \mathbf{b} = \left(\Psi_M^T\right)^{-1} \mathbf{v}_b \tag{41a.b}$$

In this fully determined case, the matrix equation for physical co-ordinates in equation (31) can be transformed to equation (40) for modal co-ordinates using the co-ordinate transform relations given in equations (35) and (41). The transformed matrices are $\overline{\mathbf{Z}}_m = \Psi_M \mathbf{Z}_m \Psi_M^T$, $\overline{\mathbf{H}} = \Psi_M \mathbf{H} \Psi_M^T$, and $\overline{\mathbf{Z}}_b = \Psi_M \mathbf{Z}_b \Psi_M^T$. The matrix $\overline{\mathbf{Z}}_e$ can be obtained from either $\overline{\mathbf{Y}}_e^{-1}$ or $\Psi_M \mathbf{Z}_e \Psi_M^T$.

This section has discussed a general formulation to the analysis of a flexible equipment structure on a set of mounts. Due to the fully populated transformed mount impedance and controller matrices, an analytical study on mechanical coupling and control mechanisms is difficult. As was shown with a single mount system in the previous section, flexible vibration on the equipment structure may cause instability when it is strongly coupled with the base. Thus, an equipment structure of 3-dimensional but rigid will be considered in the next section.

4.2 Rigid equipment

This section considers a simple but practically important case where a three-dimensional rigid equipment structure is installed on a flexible base structure through four mounts as shown in Figure 12. In this case, the number of mounts is greater than the number of equipment modes i.e., $M > N$ (overdetermined in equation (35)) where N is three: one displacement and two rotations. Rather than using the kinetic energy formulation given in equation (34), it is more convenient to describe it in terms of the equipment inertia matrix $\mathbf{J}_e$ as follows:

$$E_k = \frac{1}{2}\mathbf{a}^{\mathrm{H}}\mathbf{J}_e\mathbf{a} \tag{42}$$

where $\mathbf{a} = \{\dot{w} \quad \dot{\theta} \quad \dot{\phi}\}^{\mathrm{T}}$ denoting the heave, pitch and roll velocities at the mass centre. The inertia matrix of the equipment is $\mathbf{J}_e = \overline{\mathbf{Z}}_e / j\omega$, and is written as

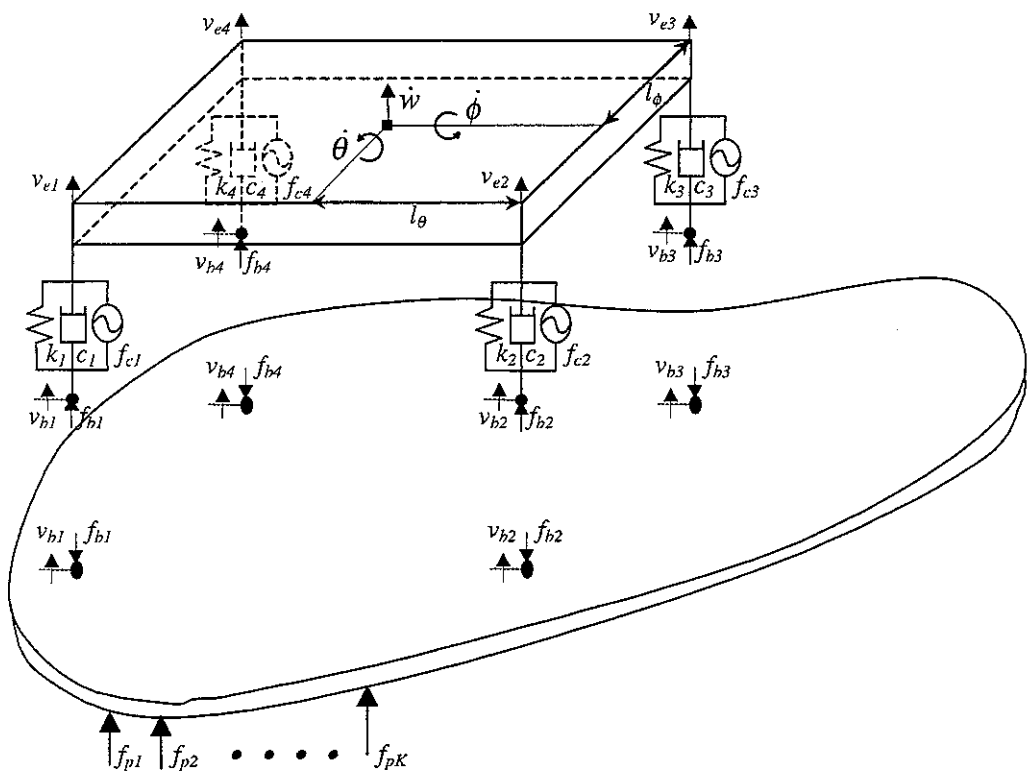

Figure 12. A 3-dimensional isolator sitting on a flexible base structure through the 4 mount supports

$$\mathbf{J}_e = \begin{bmatrix} M_e & 0 & 0 \\ 0 & J_\theta & 0 \\ 0 & 0 & J_\phi \end{bmatrix} \tag{43}$$

where M_e is the total mass of the equipment, I_θ and I_φ are the moment of inertia to pitch and roll motions, respectively. The difference between equations (34) and (42) is due to the different mode normalising factors. In a similar way to the transform relationship in equation (35), the new modal transformation matrix denoted $\mathbf{Q}$ satisfies

$$\mathbf{v}_e = \mathbf{Q}\mathbf{a}, \qquad \mathbf{a} = \mathbf{R}\mathbf{v}_e \tag{44,45}$$

where $\mathbf{v}_e = \{v_{e1} \quad v_{e2} \quad v_{e3} \quad v_{e4}\}^T$ is the nodal velocity vector. Since equation (44) is over-determined, the pseudo-inverse of $\mathbf{Q}$ can be obtained from its least square solution to account for measurement errors in the velocity signals so that $\mathbf{R} = (\mathbf{Q}^T\mathbf{Q})^{-1}\mathbf{Q}^T$ [17,18]. Thus rewriting equation (38) in terms of $\mathbf{a}$ but without feedback control gives

$$\begin{bmatrix} \overline{\mathbf{Z}}_e + \overline{\mathbf{Z}}_m & -\mathbf{Q}^T\mathbf{Z}_m \\ -\mathbf{Z}_m\mathbf{Q} & \mathbf{Z}_b + \mathbf{Z}_m \end{bmatrix} \begin{Bmatrix} \mathbf{a} \\ \mathbf{u}_b \end{Bmatrix} = \begin{Bmatrix} \mathbf{g}_c \\ \mathbf{d}_p - \mathbf{f}_c \end{Bmatrix} \tag{46}$$

where the generalised control force vector is $\mathbf{g}_c = \mathbf{Q}^T\mathbf{f}_c$, and $\overline{\mathbf{Z}}_m = \mathbf{Q}^T\mathbf{Z}_m\mathbf{Q}$ is the modal mount impedance matrix which is the transformed form of the nodal mount impedance matrix $\mathbf{Z}_m$. When velocity feedback control with the control gain matrix $\mathbf{H}$ is applied, the control force vector is written as

$$\mathbf{f}_c = -\mathbf{H}\mathbf{v}_e \tag{47}$$

Since $\mathbf{g}_c = \mathbf{Q}^T\mathbf{f}_c$ and $\mathbf{v}_e = \mathbf{Q}\mathbf{a}$, the modal gain matrix is written as

$$\overline{\mathbf{H}} = \mathbf{Q}^T\mathbf{H}\mathbf{Q} \tag{48}$$

Using equations (46) and (48), the active system can be written as

$$\begin{bmatrix} \overline{\mathbf{Z}}_e + \overline{\mathbf{Z}}_m + \overline{\mathbf{H}} & -\mathbf{Q}^T\mathbf{Z}_m \\ -(\mathbf{Z}_m + \mathbf{H})\mathbf{Q} & \mathbf{Z}_b + \mathbf{Z}_m \end{bmatrix} \begin{Bmatrix} \mathbf{a} \\ \mathbf{u}_b \end{Bmatrix} = \begin{Bmatrix} \mathbf{0} \\ \mathbf{d}_p \end{Bmatrix} \tag{49}$$

Equation (49) is a compact description of the four-mount active vibration isolation system in terms of impedance. Note this is also a simple extension form of the single mount system in equation (9). The solution of equation (49) can be obtained by inverting the impedance matrix, provided the system is stable. If the perfect control force vector $\mathbf{f}_{co} = -\mathbf{Z}_m\mathbf{v}_b$ is applied, it uncouples the mounted equipment from the vibrating base structure so that the active system becomes similar to equation (11).

Rather than implementing a complex 4-input 4-output fully coupled control system, it is interesting to consider the simplified system when four separate SISO (single-input-single-output) control systems are used. In this case the control gain matrix **H** becomes diagonal. This is termed as *decentralised control* [10,11] where each of the four actuators is controlled *independently* by feeding back the corresponding equipment absolute velocity response at the same location. For the symmetrically installed equipment structure as shown in Figure 12, the transform matrices are given by

$$\mathbf{Q}=\begin{bmatrix} 1 & -l_\theta & -l_\phi \\ 1 & +l_\theta & -l_\phi \\ 1 & +l_\theta & +l_\phi \\ 1 & -l_\theta & +l_\phi \end{bmatrix}, \qquad \mathbf{R}=\frac{1}{4}\begin{bmatrix} 1 & 1 & 1 & 1 \\ -1/l_\theta & +1/l_\theta & +1/l_\theta & -1/l_\theta \\ -1/l_\phi & -1/l_\phi & +1/l_\phi & +1/l_\phi \end{bmatrix} \tag{50,51}$$

If it is assumed that the installation of the equipment is statically balanced [1] so that $\overline{\mathbf{Z}}_{\mathbf{m}}$ is diagonal, then for the symmetrical system shown in Figure 12 the impedances of each mount are the same Z_m. If it is further assumed that the gains of each controller are the same H, the equipment dynamic equation given in the (1,1) term of equation (49) becomes diagonal, and is given by

$$\overline{\mathbf{Z}}_{\mathbf{e}}+\overline{\mathbf{Z}}_{\mathbf{m}}+\overline{\mathbf{H}}=\begin{bmatrix} j\omega M_u+Z_m+H & 0 & 0 \\ 0 & j\omega J_\theta+(Z_m+H)l_\theta^2 & 0 \\ 0 & 0 & j\omega J_\phi+(Z_m+H)l_\phi^2 \end{bmatrix} \tag{52}$$

The equipment dynamic equations are uncoupled even after control, and the gain H is simply added to the mount impedance Z_m in all three motions. This means that, for the statically balanced symmetric structure as shown in Figure 12, the use of a single common gain for decentralised control (*equi-decentralised control*) results in the modal controller (*equi-modal control*) equivalently reducing all modes. Each of four control forces has the same effect as a skyhook damper, as far as the relative equipment motions are concerned as discussed in Section 2.1. The four skyhook dampers at each mount location can equivalently reduce every rigid body mode of the equipment structure. Consider the general case when the equipment structure is non-symmetric but statically balanced as is preferred in practice [1]. Equi-modal control can again be achieved by making the modal control gain matrix $\overline{\mathbf{H}}$ diagonal similarly as $\overline{\mathbf{Z}}_{\mathbf{m}}$.

When only some of the four actuators are working, one can easily analyse the system using the relationship $\overline{\mathbf{H}}=\mathbf{Q}^{\mathrm{T}}\mathbf{H}\mathbf{Q}$ but setting to zero to the diagonal terms of **H** for non-working mount forces. Since four actuators are used to control three modes, one is

redundant and three actuators may be sufficient. If only two actuators are applied, for example, mount number 1 and 2 in Figure 12, then the control system may not be able to control the roll motion $\dot{\phi}$.

4.3 Stability analysis of the four-mount system

This section considers stability analysis of the active vibration isolation system for the 3-dimensional rigid equipment as shown in Figure 12. The 4-input 4-output multichannel feedback control system can be represented as a general block diagram for disturbance rejection as shown in Figure 13. The multichannel plant matrix $\mathbf{G}(j\omega)$ is of size (4×4) and is give by

$$\mathbf{v}_e = \mathbf{G}(j\omega)\mathbf{f}_c \tag{53}$$

Stability of the multichannel system can be determined from the open loop frequency response function matrix $\mathbf{L}(j\omega) = \mathbf{G}(j\omega)\mathbf{H}$ using the generalised Nyquist criterion[10], which states that the closed loop system is stable provided none of the eigenvalue loci of $\mathbf{L}(j\omega)$ should encircle the $(-1, 0)$ point in the complex plane. If equi-decentralised control is implemented with a common gain H, $\mathbf{L}(j\omega)$ can be written as

$$\mathbf{L}(j\omega) = H\mathbf{G}(j\omega) \tag{54}$$

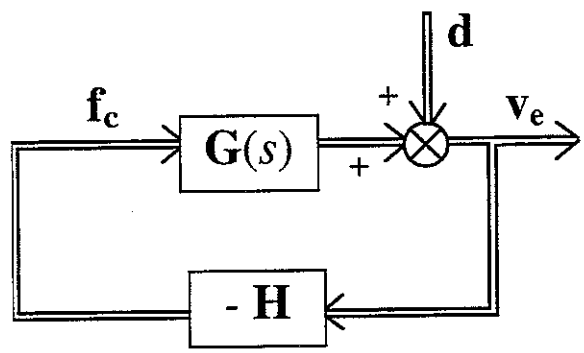

Figure 13. Multichannel feedback control system for disturbance rejection

None of the eigenvalue loci of $\mathbf{G}(j\omega)$ encircle the $(-1, 0)$ point for *stability*, and none of the eigenvalue loci should cross the negative real axis for *unconditionally stability*. Because one of the responses in $\mathbf{v}_e$ is linearly dependent on the others and thus one of the eigenvalues is zero, it is thus convenient to judge the criterion for unconditional stability in the transformed co-ordinates as [17,18]

$$eig(\mathbf{RG}(j\omega)\mathbf{Q}) \tag{55}$$

The plant matrix can be obtained by solving equation (46) with $\mathbf{d}_p = \mathbf{0}$ and using the transform relation in equation (44). It is generally non-symmetric due to non-symmetric installation of the mounted equipment on the base.

The stability of the decentralised control system with a common gain H can be assessed analytically. Consider first the case when either the mounted equipment-base system is weakly coupled or the control actuators are only acting on the equipment structure. Each pair of input and output is collocation control, because each plant is the driving point mobility. Each independent control system is unconditionally stable. When all of the controllers are acting with a common gain H, the stability can be tested by examining $\mathbf{G}(j\omega)$ using equation (55). The plant $\mathbf{G}(j\omega)$ is square symmetric, and is the mobility matrix of a mechanical system. The real part of the eigenvalues of the plant matrix is positive for the mechanical system to be a passive(power absorbing) mechanical device. By definition, the passive mechanical system is assumed to be passive. Thus when a multichannel control system has the driving point input mobility matrix as its plant, it is unconditionally stable to the change of the common gain H [6,7].

Now we examine the strongly coupled case particularly when the co-ordinate transformations are fully determined i.e. $\mathbf{Q}$ in equation (44) is square and invertible, such as the two mount system with a two-dimensional equipment and the three mount system with a three-dimensional equipment. In this case, the transform matrix in equation (45) is $\mathbf{R} = \mathbf{Q}^{-1}$, and the same co-ordinate transform relations can be also applied to the base velocity vector as

$$\mathbf{v}_b = \mathbf{Q}\mathbf{b}, \qquad \mathbf{b} = \mathbf{R}\mathbf{v}_b \tag{56,57}$$

where $\mathbf{b}$ is the transformed base velocity vector. By setting $\mathbf{d}_p = \mathbf{0}$ in equation (46) and using these relations, the plant matrix is given by

$$\mathbf{G}(j\omega) = \mathbf{Q}\left(\overline{\mathbf{Z}}_e + \overline{\mathbf{Z}}_m + \overline{\mathbf{Z}}_m \overline{\mathbf{Y}}_b \overline{\mathbf{Z}}_e\right)^{-1} \mathbf{Q}^T \tag{58}$$

where $\overline{\mathbf{Y}}_b = \overline{\mathbf{Z}}_b^{-1}$ in which the transformed base impedance is $\overline{\mathbf{Z}}_b = \mathbf{Q}^T \mathbf{Z}_b \mathbf{Q}$. Note this is also a simple extension form of the single mount system in equation (13). Again a rigid equipment and massless mounts are assumed together with the statically balanced installation of the mounted equipment. Since $\mathbf{Q}^T\mathbf{Q} = \mathbf{I}$, applying the criterion in equation (55) gives

$$eig\left(\left(\overline{\mathbf{Z}}_e + \overline{\mathbf{Z}}_m + \overline{\mathbf{Z}}_m \overline{\mathbf{Y}}_b \overline{\mathbf{Z}}_e\right)^{-1}\right) \tag{59}$$

where $\overline{\mathbf{Z}}_e$, and $\overline{\mathbf{Z}}_m$ are diagonal, and $\overline{\mathbf{Y}}_b$ is symmetric but non-diagonal. The condition is determined by $eig\left(\overline{\mathbf{Z}}_e + \overline{\mathbf{Z}}_m + \overline{\mathbf{Z}}_m \overline{\mathbf{Y}}_b \overline{\mathbf{Z}}_e\right)$, and since the strictly positive definite characteristic of $\mathrm{Re}\left(eig(\overline{\mathbf{Z}}_e)\right) \geq 0$ and $\mathrm{Re}\left(eig(\overline{\mathbf{Z}}_m)\right) \geq 0$, it is determined by the last term $eig\left(\overline{\mathbf{Z}}_m \overline{\mathbf{Y}}_b \overline{\mathbf{Z}}_e\right)$, where $\mathrm{Re}\left(eig(\overline{\mathbf{Y}}_b)\right) \geq 0$ again due to the positive definite characteristic. If we assume there is no damping in the mounts, then the diagonal matrix $\overline{\mathbf{Z}}_m \overline{\mathbf{Z}}_e \geq 0$, whose diagonal terms are positive real and similar to that for the single mount system in Section 3.1. Thus $\mathrm{Re}\left(eig(\overline{\mathbf{Z}}_m \overline{\mathbf{Y}}_b \overline{\mathbf{Z}}_e)\right) \geq 0$, and consequently the real eigenvalues of the plant in equation (59) becomes positive definite so that $\mathrm{Re}\left(eig(\mathbf{RG}(j\omega)\mathbf{Q})\right) \geq 0$. Similarly as for the single mount system, damping in the mounts does not threaten the unconditional stability. However, if there is a flexible mode in the equipment structure, $\mathrm{Re}\left(eig(\overline{\mathbf{Z}}_m \overline{\mathbf{Z}}_e)\right)$ is no longer positive definite. Thus the system is unconditionally stable at all frequencies, provided the equipment behaves as a rigid body and the mounts as springs and dampers.

When the system is over-determined as in the four-mount system in Figure 12, there is a redundant passive mount and a redundant active force. It is thus no longer possible to apply the convenient transforms for the base responses in equations (56) and (57). The analytical plant matrix expression can still be obtained from using equation (46), but is very complex in this case. Its analytical proof is thus not given but instead some supporting simulation and experimental results in the next section.

5. Active vibration isolation of a four-mount system

5.1 Description of the system

To support the theoretical results, some computer simulations as well as experiments were conducted with the low frequency active vibration isolation model as shown in Figure 12. The three dimensional rigid equipment was installed on a flexible base structure upon four passive mounts as shown in Figure 14. The equipment structure was assumed to be uniform and rigid. The heave w, pitch θ, and roll ϕ motions are denoted at the mass centre. The locations of the four mounts are referred as Nodes 1, 2, 3, and 4 for convenience. They were assumed to have the same mechanical properties and each mount was assumed to be modelled as a parallel connection of spring k_m and damper c_m without mass. The base structure of dimensions $L_x \times L_y$ was assumed to be of free-free-clamped-clamped boundary conditions. The flexible base structure was excited by white noise from a primary force f_p, and its location is shown in Figure 14. Relevant physical and geometrical properties for simulations are tabulated in Tables 1 and 2.

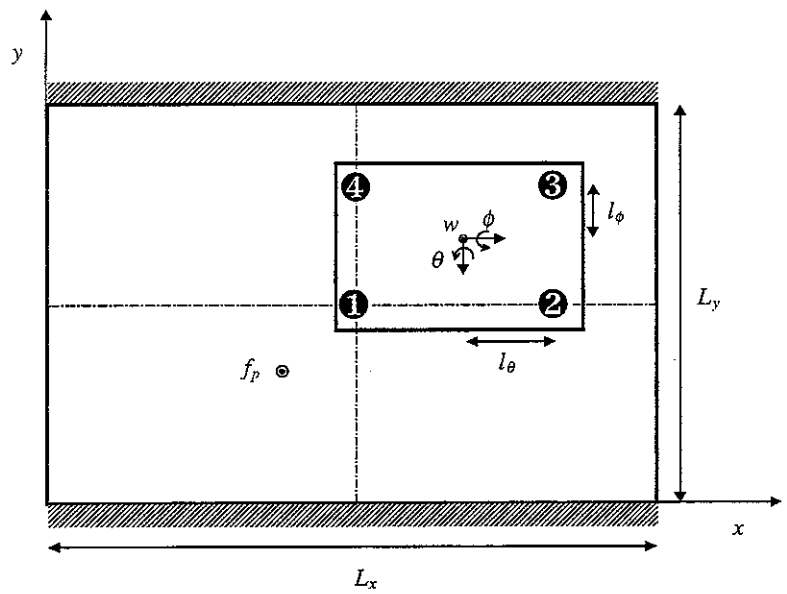

Figure 14. Schematic diagram of the active isolation system on a free-free-clamped-clamped base plate structure. The locations of the four mounts are marked as Nodes 1,2,3, and 4.

Table 1. Physical properties

Equipment Structure	M_u, Mass	6.232 kg
	I_θ, Moment of inertia to pitch motion	0.0685 kgm^2
	I_ϕ, Moment of inertia to pitch motion	0.0162 kgm^2
	Material of the equipment plate	Aluminium
Mount	k_m, Spring constant of each mount	4.2×10^4 N/m
	c_m, Damping of each mount	25.6 Ns/m
	Damping ratio to heave (w), pitch (θ), and roll (ϕ) motions	$\zeta_w = 0.05$ $\zeta_\theta = 0.056$ $\zeta_\phi = 0.046$
Base Plate	Material	Steel
	ζ, Damping ratio	0.01

Table 2. Geometric data

($L_x\times L_x\times t$), Dimensions of the steel base plate (mm)	$(700\times500\times2)$
($L_x\times L_x\times t$), Dimensions of the aluminium equipment plate (mm)	$(300\times160\times20)$
Mount locations on the equipment (mm)	$l_\theta = 117,\ l_\theta = 47$
Location of the primary force (mm)	(320, 270)
Location of Node 1	$(L_x/2, L_y/2)$

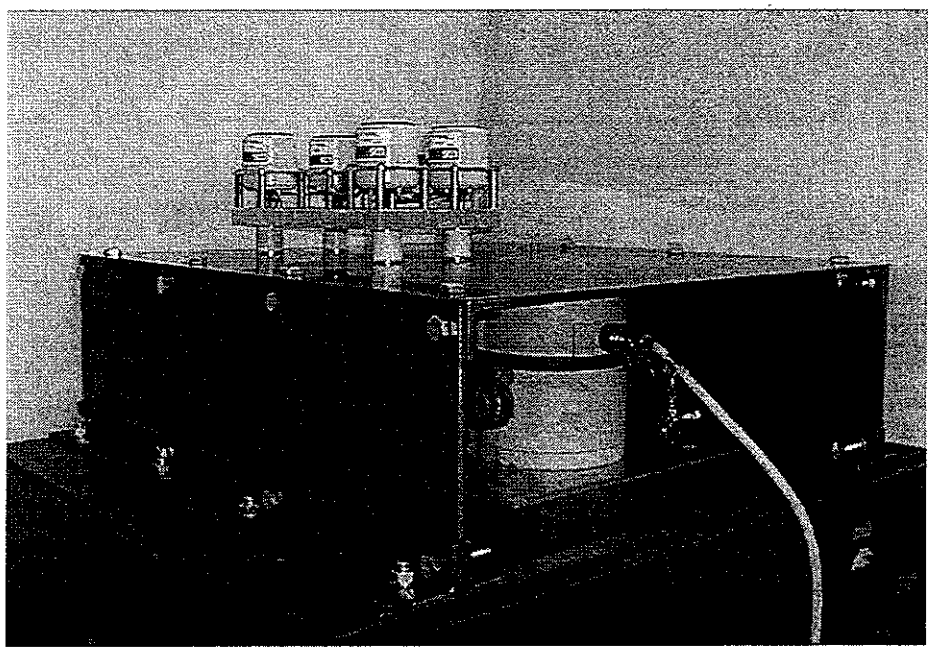

Figure 15. Experimental set-up

For a comparison with experiments, the simulation model shown in Figure 14 was physically fabricated as shown in Figure 15. The large shaker underneath the rectangular plate was the primary force actuator, and a mounted equipment structure was installed on top of the free-free-clamped-clamped plate. Two facing sides of the plate were bolted on stiff frames to realise the clamped-clamped boundary conditions. The equipment structure was a combined structure between four electromagnetic actuators and a thick aluminium plate of thickness 20 mm, and was supported by four mounts as shown in Figure 15. In order to realise the parallel installation of actuators with the mounts as shown in Figure 12, the four actuators were fixed on the thick equipment plate and were located on top of each mount position. The detailed structure of each active isolation system is shown in Figure 16 where a stinger is connected between the actuator and the mount foot through the mount. The same realisation could be achieved by fixing the actuator now on the flexible base and connecting the stinger to the equipment plate. However, the first configuration was chosen for convenience of base vibration analysis as well as for making the mounted equipment and base structures strongly coupled. The mount was made of natural rubber that was moulded to be of hollow cylinder shaped. The locations of the mounts on the plate is shown in Figure 14, and the physical and geometric properties for the experimental set-up are the same as those for simulations shown in Tables 1 and 2.

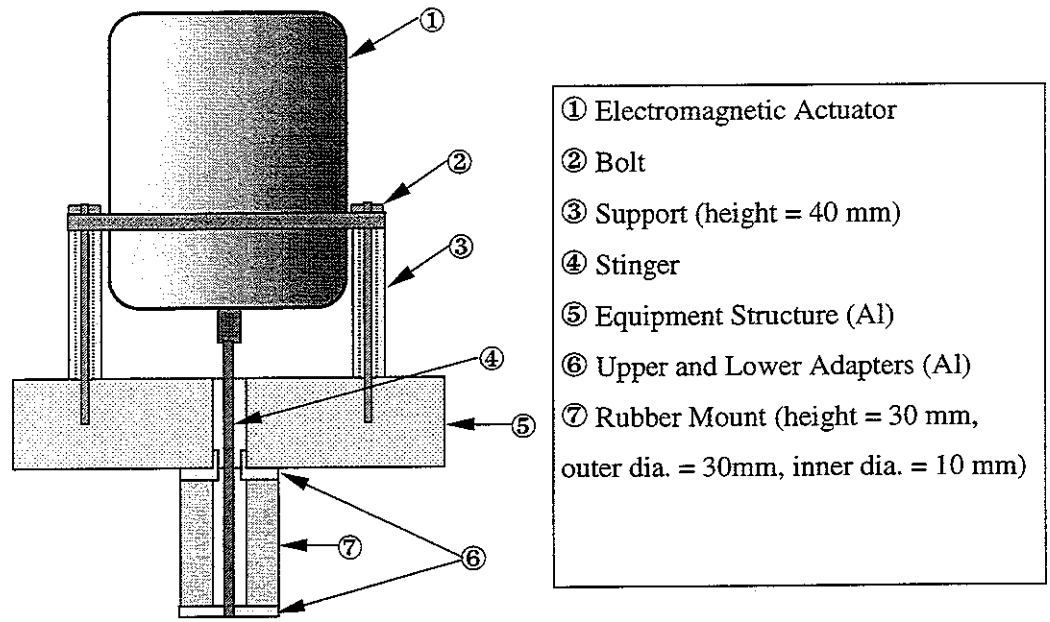

Figure 16. Structure of the active isolator

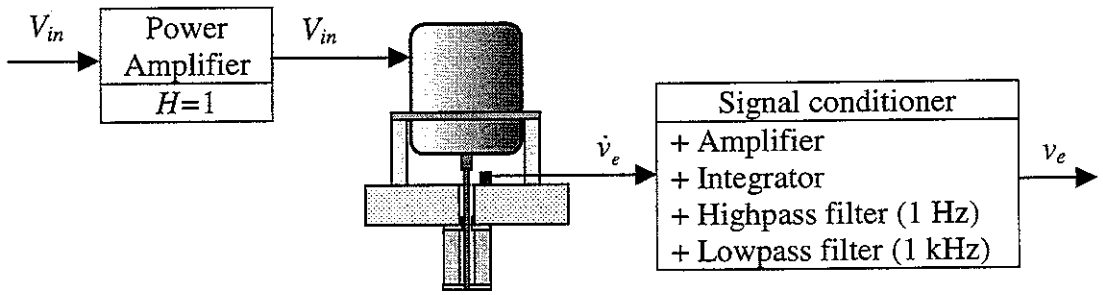

Figure 17. Plant response measurement for a single plant

5.2 System identification and stability test

Before any control technique is applied, identification of the experimental plant is useful for stability analysis as well as validation of the theoretical model. The mounted equipment structure was first installed on a rigid base structure to identify the uncoupled characteristics of the structure itself. The measurement system is shown in Figure 17 for a single channel. The input voltage V_{in} to the electromagnetic actuator was measured and used as the input signal instead of the input force. It was because, at low frequencies the input voltage is approximately proportional to the input current that is directly

proportional to the force input[19]. In addition, velocity of the equipment was obtained from first measuring acceleration by using a piezo-type accelerometer and then passing it through an integrator. The integrator was an integrated module inside a general signal conditioner used (B&K type 2635) as shown in Figure 17, and was operated in conjunction with a highpass filter in order to avoid instability at 0 Hz. The cutoff frequency of the highpass filter was set to be 1 Hz. The signal over than 1 kHz was again filtered by using a lowpass filter so as to assure that only the rigid body modes of the equipment are measured. Figure 18(a) shows a plant response when the actuator at Node 1 was excited and the equipment velocity response at the same location was measured. Since the frequency response function is the sensor response at Node 1 to the excitation at Node 1, it is corresponding to the plant G_{11}. The plant G_{11} is the (1,1) element of the plant matrix $\mathbf{G}(j\omega)$ in equation (53). For comparison, experimental (solid line) and simulation (dashed line) results are shown together. The experimental result below 5 Hz had poor coherence due to low sensitivity of the actuator and sensor used, and resulted in some discrepancy compared with the prediction in Figure 18(a). It should be noted that in the predicted plant, perfect operation of the power amplifier and the integrator was implicitly assumed with no measurement noise. Except the frequency range under 5 Hz, however, the experimental result in Figure 18(a) agrees well with the prediction. The three rigid body modes are around 25 Hz as shown in Table 3, and whose passive damping ratios are around 5 % as listed in Table 1.

The mounted equipment structure was then installed on the flexible structure as shown in Figure 14, and the plant G_{11} was measured. The same measurement configuration as for the rigid base case was used as shown in Figure 17. The plant response is now a coupled response between the mounted equipment and base structures, and the experimental (solid) and simulation (dashed) results are shown in Figure 18(b). The first three dominant peaks around 20 Hz are corresponding to heave motion at 15.8 Hz, pitch motion at 21.3 Hz, and roll motion at 22.5 Hz. The peaks at frequencies over about 30 Hz clearly show the influence of the flexible base structure. The experimental result agrees reasonably well with the simulation under 30 Hz, where the response is dominated by the uncoupled mounted equipment. Some discrepancies over 30 Hz was thought to be due to imperfect physical realisation of the clamped-clamped boundary condition of the base plate. Due to strong coupling, the uncoupled rigid body modes around 25 Hz are pushed down to around

20 Hz and the uncoupled first base mode about 35 Hz for experiment are pushed up to about 40 Hz. This phenomenon can be easily understood by coupling analysis of a simple two d.o.f system as shown in Figure 4(b)[15,16].

The frequencies are compared in Table 3 with those for the uncoupled mounted equipment. Each motion could be clearly distinguished by measuring the other plant responses and checking the phases at the natural frequencies. It is interesting to note that the order of the modes is changed when the mounted equipment is strongly coupled with the base. It is because, at those frequencies around 20 Hz the base structure acts as springs, but the spring constants for each motion are different. For example, the natural frequency for roll motion becomes the highest because it has the highest spring constant on the base to this motion.

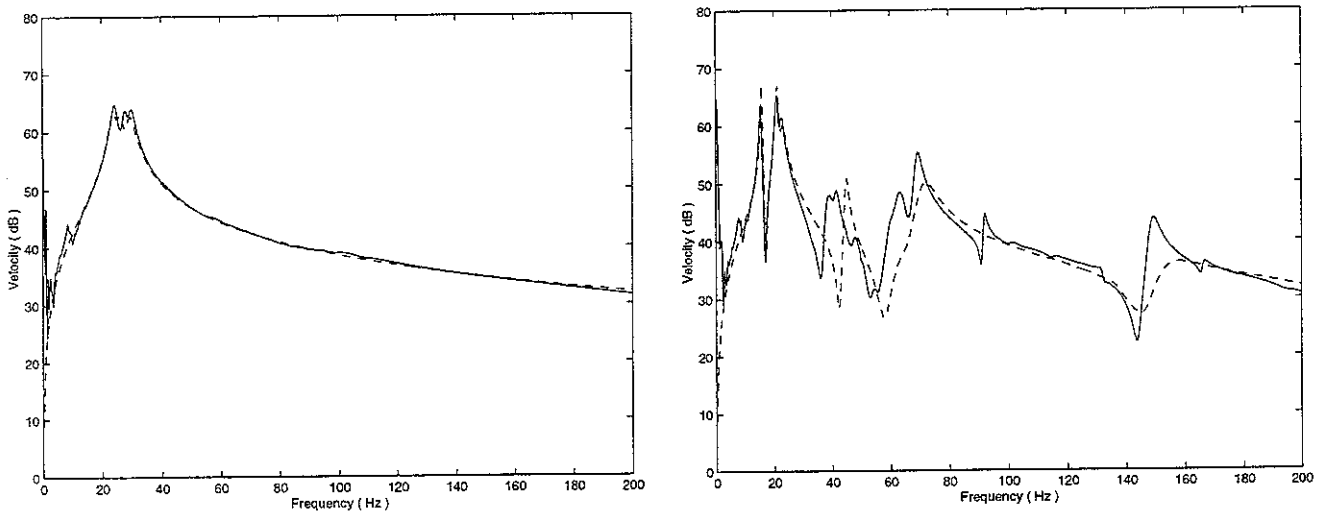

(a) G_{11} on a rigid base (b) G_{11} on the flexible base

Figure 18. Plant responses at Node 1 when the actuator at Node 1 is active. (dB ref.=10^{-5} m/s)

Table 3. Natural frequencies of the system

Cases \ Motions	Heave, $\dot{w}$	Pitch, $\dot{\theta}$	Roll, $\dot{\phi}$
Uncoupled mounted equipment	26 Hz	29 Hz	24 Hz
Coupled mounted equipment	15.8 Hz	21.3 Hz	22.5 Hz

The other plant responses were also calculated and measured to construct the whole plant matrix $\mathbf{G}(j\omega)$. With the complete plant matrix, stability were assessed by applying the generalised Nyquist criterion discussed in Section 4.3. The resulting eigenvalue loci are shown in Figure 19(a) and 19(b) for the theoretical and experimental models respectively. Solid line denotes the locus of heave mode, and dashed and dotted lines denote the loci of pitch and roll motions respectively. Figure 19(a) clearly shows that none of the eigenvalue loci from the simulation crosses the negative real axis. The loci from the experimentally measured plant are shown in Figure 19(b). The plot does not clearly show whether or not they cross the negative real axis near the origin, especially at very low frequencies less than 5 Hz where the plant was suffered from noise due to low coherence. The low frequency behaviour is discussed in detail in Section 6. Nevertheless, most portions of the loci are in the right-half plant, and are very similar to those from the predicted plants.

Stability of a control system, where only some of the actuators, are working can be assessed by using a corresponding sub-matrix of the given whole plant matrix. The predicted plant matrix was used and the resulting eigenvalue loci are shown in Figure 20; for one working actuator at Node 1 in Figure 20(a), for two working actuators at Nodes 1 and 2 in Figure 20(b), and for three working actuators at Nodes 1, 2, and 3 in Figure 20(c). The results show that none of the eigenvalue loci cross the negative real axis in none of the cases. It demonstrates that, as long as the driving point mobility-like plant is unconditionally stable, its sub-matrices are also unconditionally stable for the simulations considered here.

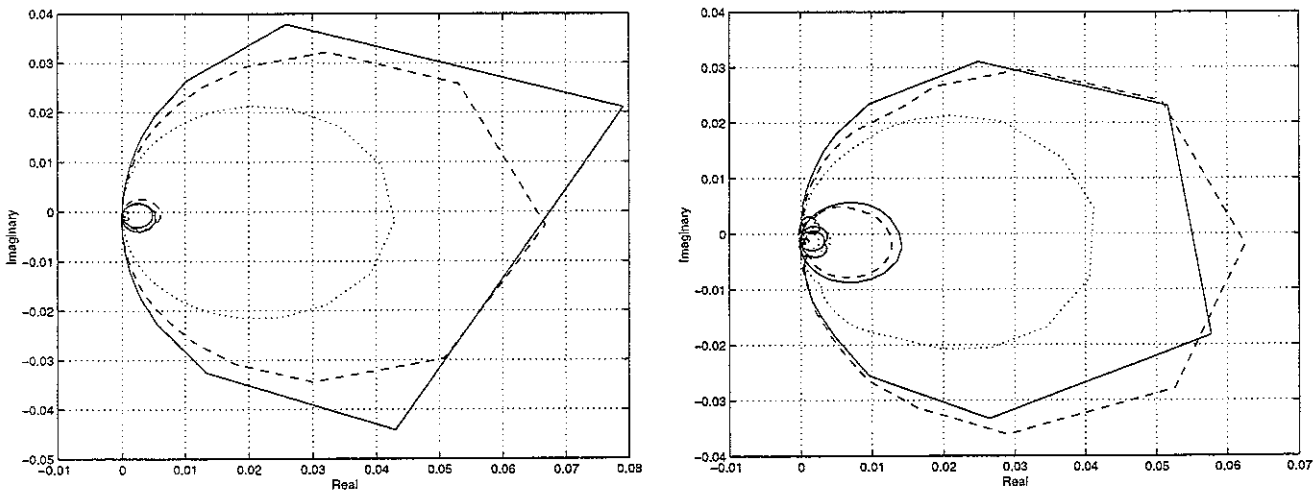

(a) prediction (b) experiment

Figure 19. Eigenvalue loci of the plant on the flexible base structure when all four actuators are active; heave(solid), pitch(dashed), and roll(dotted).

(a)

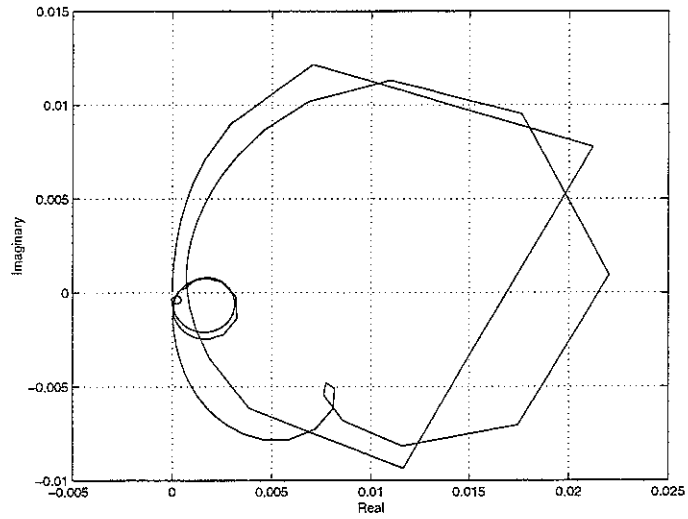

(b)

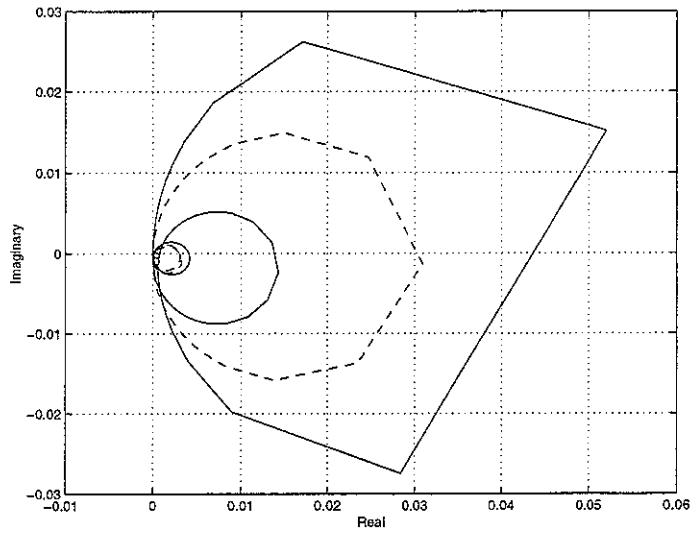

(c)

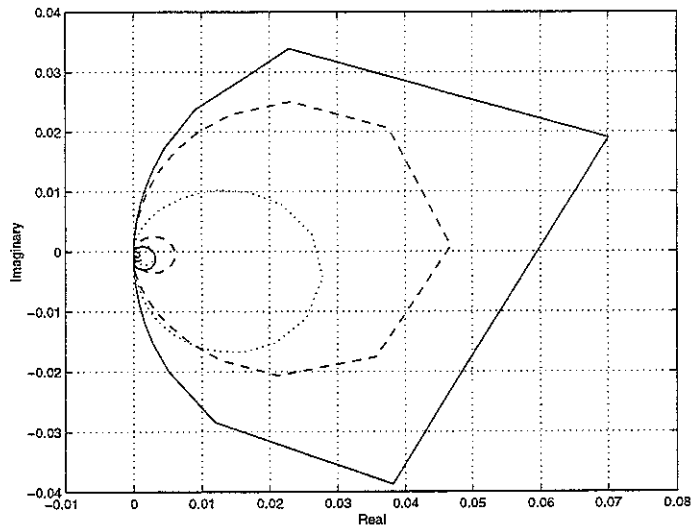

Figure 20. Eigenvalue loci of the plant on the flexible base structure; (a) Actuator at Node 1 is active. (b) Actuators at Nodes 1 and 2 are active, (c) Actuators at Nodes 1, 2, and 3 are active; heave(solid), pitch(dashed), and roll(dotted).

5.3 Control performance

This section examines control performance of equi-decentralised control according to the change of control gain. Control performance in the predicted model is first considered. The flexible base plate in Figure 14 was assumed to be excited by white noise, and a common gain H was used to control each independent SISO control system. The nodal equipment velocity responses at each mount position are shown in Figure 21, where responses before control are shown with solid lines and those after control are shown with dashed lines. In Figure 21(a), the highest response (solid line) is the response at Node 1 before control, and the others (dashed lines) are corresponding to gains 110, 320, 1000, 3350, 10000 from high to low response order. It clearly shows that, as the gain increases, the vibration amplitude is gradually reduced almost all over the frequency range. The trend is the same for the nodal responses at Nodes 2, 3, and 4. Some amplification near 30 Hz at Node 2 is due to the redundancy of the control configuration that uses four actuators to control three rigid body modes. The modal performance was then calculated from equation (45) and then relevant kinetic energies of the equipment could be obtained from equation (42). The total kinetic energy is shown in Figure 22(a), and the kinetic energies of heave, pitch, and roll motions are shown in Figure 22(b), (c), and (d) respectively. In Figure 22(a), it is interesting to note that as the gain increases, the total energy is reduced gradually in the whole frequency range without any amplification. It means that, although there is some amplification in the nodal responses in Figure 21 due to the redundancy of the actuators, the actuators are operating in a way to reduce the total kinetic energy of the equipment at all frequencies. As discussed analytically, equi-decentralised control is the same as equi-modal control so that the kinetic energies for heave, pitch, and roll motions are equivalently reduced for each control gain as shown in Figure 22(b), (c), and (d). Although this is not shown, since the plant is unconditionally stable, use of an infinite gain resulted in perfect control in an approximation sense.

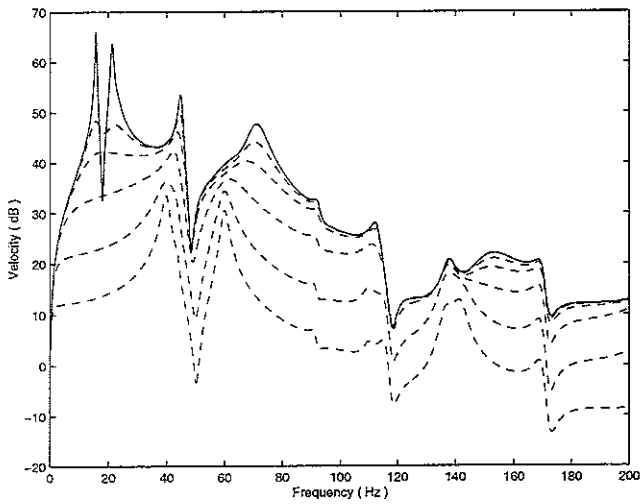

(a) Node 1

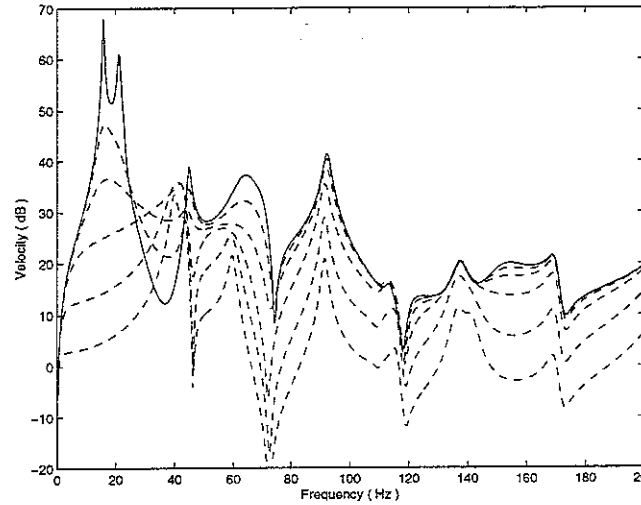

(b) Node 2

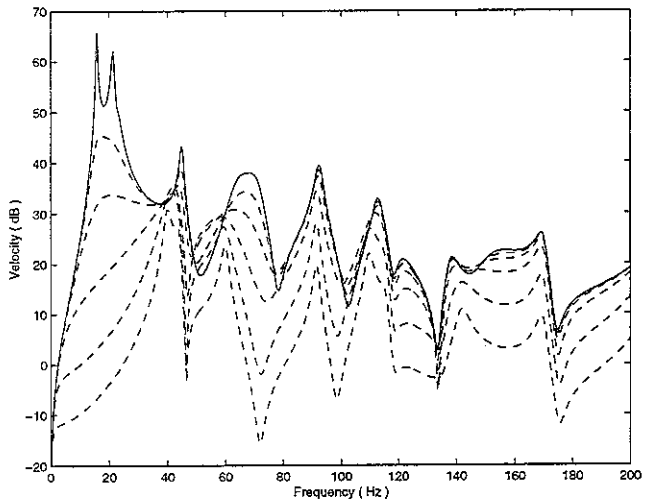

(c) Node 3

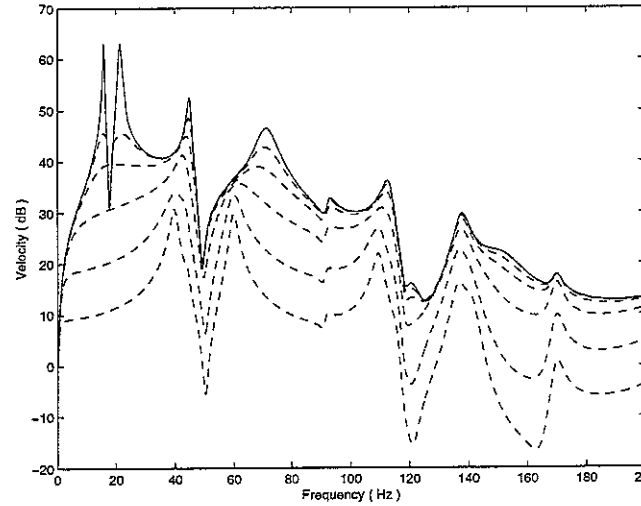

(d) Node 4

Figure 21. Simulation results of the equipment responses in physical co-ordinates; All four actuators are active. (dB ref.=10^{-5} m/s)

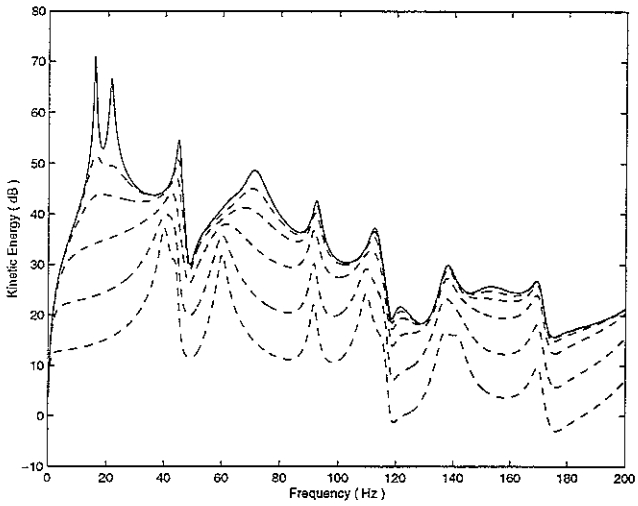

(a) Total kinetic energy

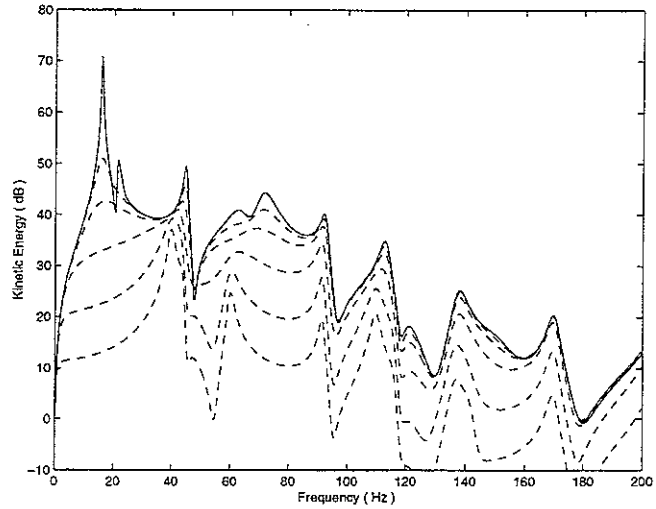

(b) Kinetic energy in heave motion, w

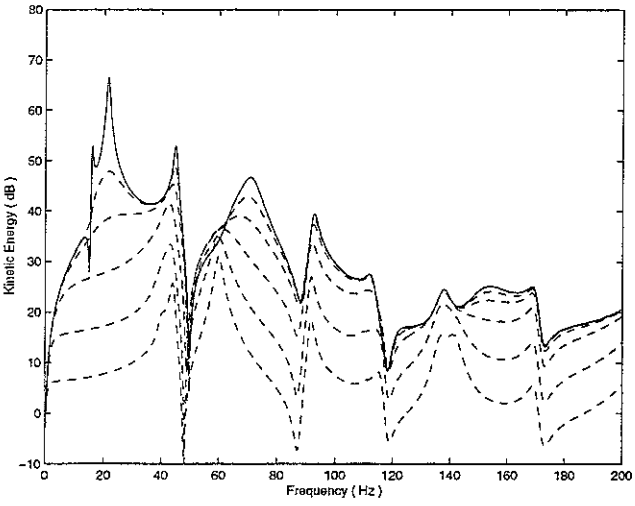

(c) Kinetic energy in pitch motion, θ

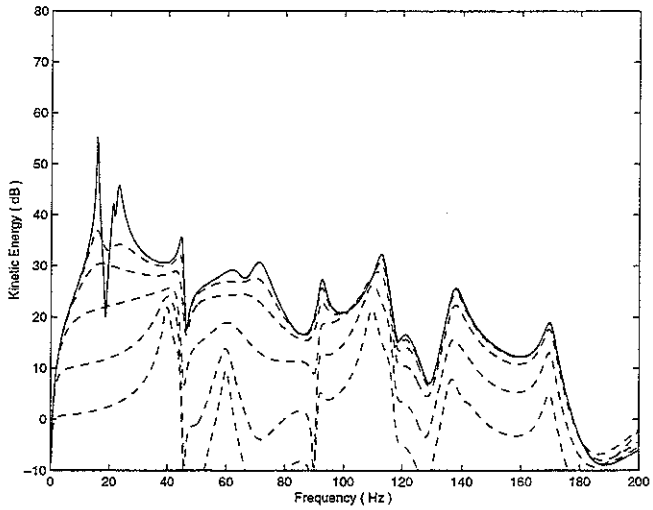

(d) Kinetic energy in roll motion, ϕ

Figure 22. Simulation results in modal co-ordinates; All four actuators are active. (dB ref.=10^{-10} J)

Control performance of the experimental plant was also examined by closing the open loop in Figure 17 and changing the control gain H. Again the flexible base plate was excited by white noise. The nodal velocity responses of the equipment are shown in Figure 23 as the same form of the prediction results shown in Figure 21. The gain values used were 110, 320 and 1000. Higher gains 3350 and 10000, which were used for predictions, could not be applied to the experimental plant. It was not because of the dynamic range of the power amplifier used, but because of instability that occurred near 1 Hz which is the cutoff frequency of the highpass filter used in conjunction with the integrator. Since the

frequency is very low where the plant response is noisy due to low sensitivity in the actuators and sensors, it was difficult to see in the eigenvalue loci plot shown in Figure 19(b). It is also difficult to see some amplification of responses under 5 Hz in Figure 23, but the very low frequency responses after control are higher than those before control. The low frequency instability is caused purely by imperfect operation of the electrical equipment used; the power amplifiers and integrators. There were some phase advances at very low frequencies in both the power amplifiers and integrators. This stability issue on practical implementation is discussed in detail in the following section. However, the experimental results above 5 Hz agree well with the predictions, even some amplification around 30 Hz especially at Node 2. As the gain increases, the velocity responses are gradually reduced. The total and individual kinetic energies are shown in Figure 24 in the same form of the predicted results shown in Figure 22. The trend above about 5 Hz is the same as that for the simulations.

To support the argument that the controller uncouples the mounted equipment from the flexible base as the gain increases, the base nodal velocity at Node 1 was calculated and also measured during control. The simulation and experimental results are shown in Figure 25(a) and (b) respectively. As the gain increases, the original base response(solid line) approaches the uncoupled base response(dotted line) that is the base response measured before installing the mounted equipment. Dashed lines correspond to the base responses for each control gain. It clearly demonstrates that the mechanism of the active isolation system; the controller uncouples the mounted equipment from the base by using the force actuators installed in parallel with each mount.

Control performances from both predictions and experiments are tabulated in Table 3 according to the gain values used. The absolute gain value H can be regarded as a skyhook damping as far as the mounted equipment dynamics are concerned. Thus it is also expressed in the table as skyhook damping and skyhook damping ratio that were calculated based on heave motion. The passive damping of a single mount is denoted as c_m, and note that the damping ratios of the passive system are about 5 % as shown in Table 1. The overall kinetic energy of the experiment was calculated from 5 Hz to 200 Hz to avoid accounting for the amplification region. Both simulation and experiment results agree well, and offer a reduction of more than 14 dB for a gain 1000.

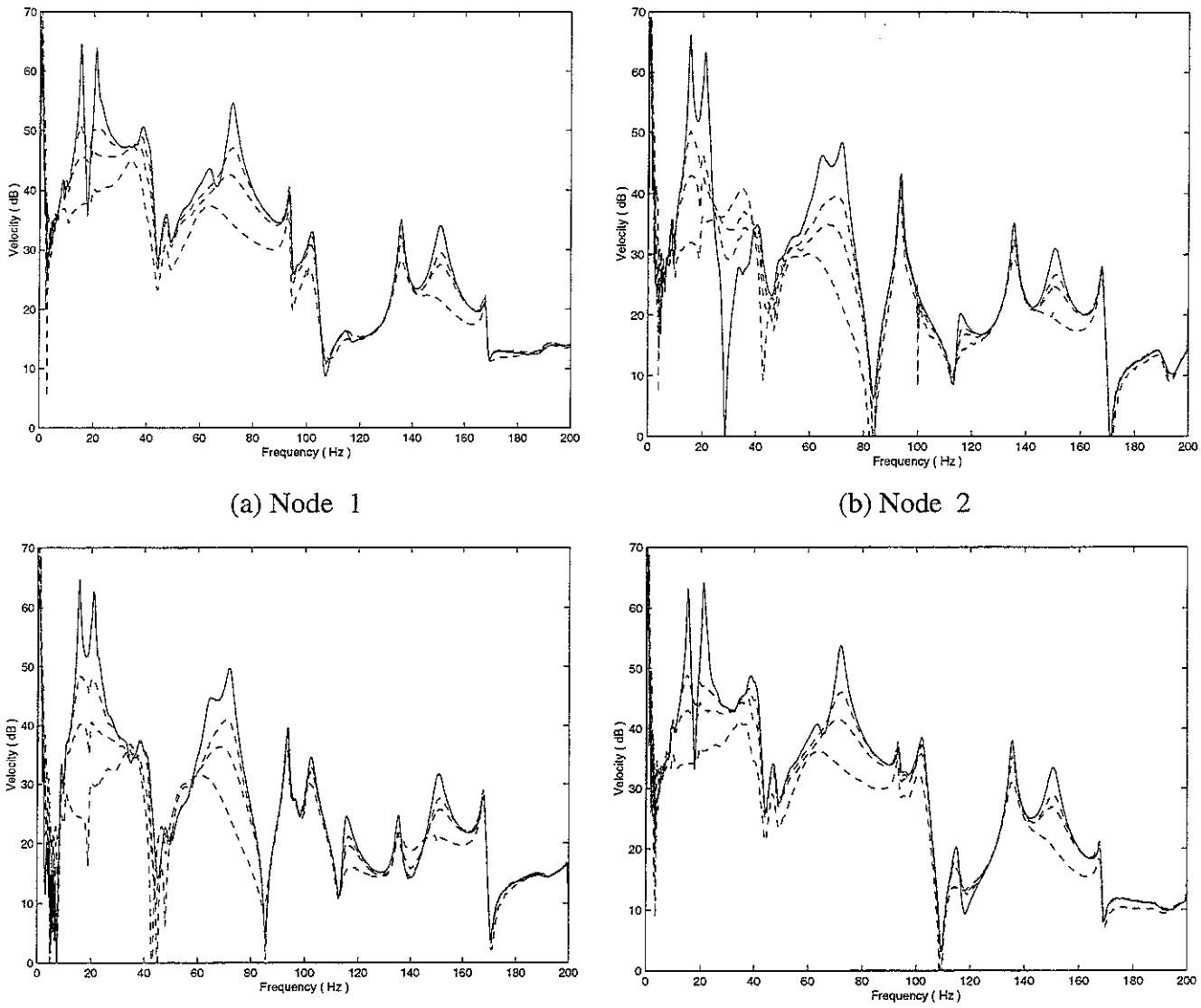

(a) Node 1

(b) Node 2

(c) Node 3

(d) Node 4

Figure 23. Experimental results in physical co-ordinates; All four actuators are active. (dB ref.=10^{-5} m/s)

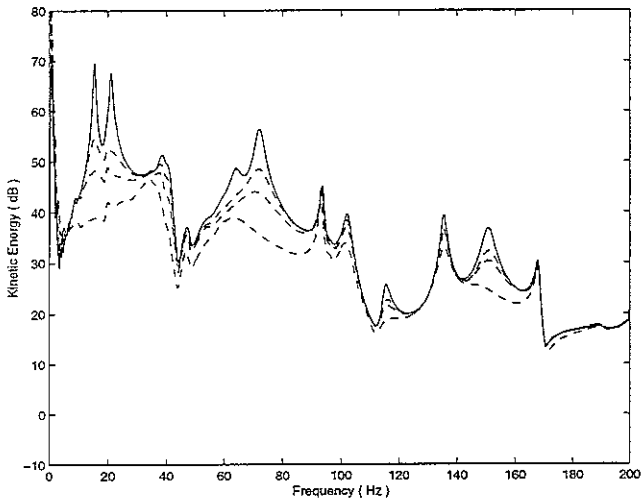

(a) Total kinetic energy

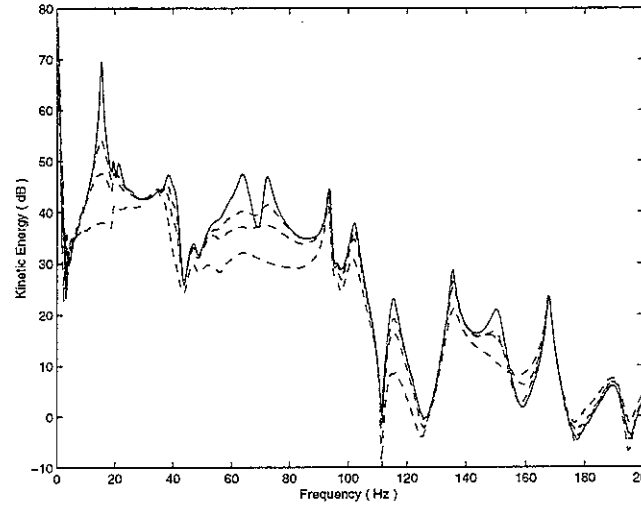

(b) Kinetic energy in heave motion, w

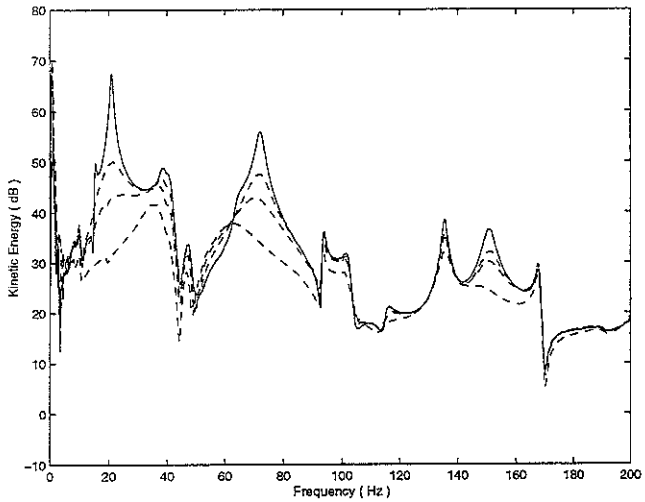

(c) Kinetic energy in pitch motion, θ

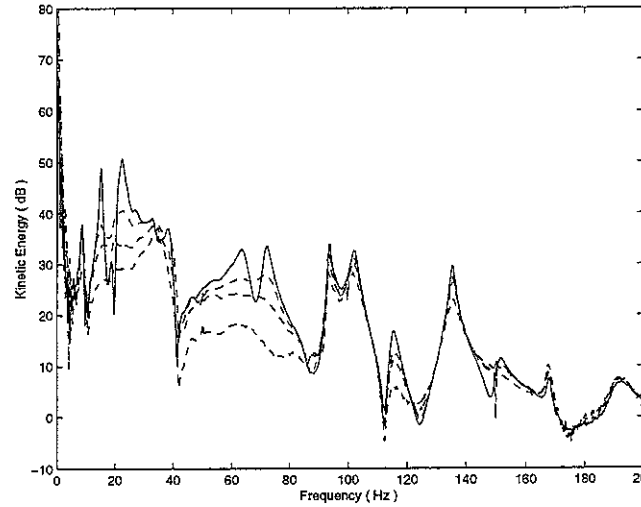

(d) Kinetic energy in roll motion, ϕ

Figure 24. Experimental results in modal co-ordinates; All four actuators are active. (dB ref.=10^{-10} J)

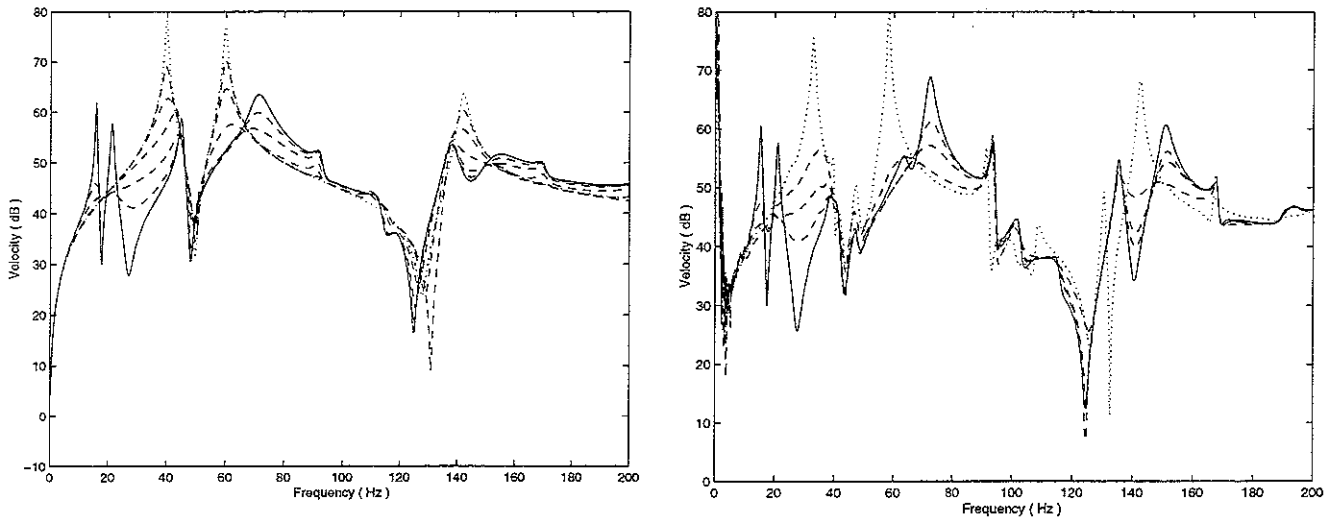

(a) Simulations (b) Experiments

Figure 25. Base response at Node 1 according to the control gains; All four actuators are active.

Table 4. Comparison of the control performances. Skyhook damping and its ratio are calculated based on the heave motion.

Gains			Energy ratio J_o/J_i (%)		Overall reduction(dB)	
Absolute Value, h	Skyhook Damping	Skyhook Damping Ratio	Theory	Experiment	Theory	Experiment
110	$4.3 \times c_m$	0.215	18.82	19.59	-7.3	-7.1
320	$12.5 \times c_m$	0.626	8.14	10.31	-10.9	-9.9
1000	$39.1 \times c_m$	1.955	3.21	4.0	-15.0	-14.0
3350	$130.9 \times c_m$	6.548	1.52	.	-18.2	.
10000	$390.6 \times c_m$	19.546	0.82	.	-20.9	.

* Experimental results are from 5 Hz to avoid the large amplification at low frequencies (especially 1 Hz which is the cutoff frequency for the highpass filter)

6. Causes of instability

This section discusses the causes of instability occurred in the experimental plant. The instability under 5 Hz in the previous section would be due to imperfect operation of electrical equipment used as shown in Figure 17, especially due to phase shift in the power amplifier and the signal conditioner. Theoretically, a phase advance of a little more than 90° at low frequencies is sufficient for the eigenvalue loci to cross the negative real axis so as to make the system unstable to a high gain [7]. The Bode plot of the power amplifier used is shown at each measured frequency in Figure 26 together with the ideal amplifier responses(dotted). In Figure 26(a), the large amplitude at 0 Hz would be the reason of large plant responses in the experimental model in the previous section. More interestingly, in Figure 26(b) the commercial amplifier shows phase advance up to about 90° at very low frequencies compared to the ideal amplifier response. The signal conditioner used(B&K type 2635) had an integrator as a module so that the characteristics of the integrator could be calculated by dividing a measured velocity response at a position by a measured acceleration response at the same location. The integrator had to be used to be combined with a highpass filter whose cutoff frequency could be set to be either 1 Hz or 10 Hz. Both cutoff frequencies were tested and the resulting Bode plots are shown in Figure 27, where the integrator with the highpass cutoff frequency 10 Hz(solid line), that with the cutoff frequency 1 Hz(dashed line), and the ideal integrator are shown together. Due to the low sensitivity of the actuator and the sensor at the very low frequencies, responses under 5 Hz had low coherence and are not shown. In Figure 27(b), the integrator with the cutoff frequency 10 Hz has about 90° phase advance near 10 Hz compared to the ideal integrator response. For the experiment in the previous section, the cutoff frequency was set to be 1 Hz. However, Figure 27(b) clearly shows that the integrator with the cutoff frequency 1 Hz also has some phase advance at very low frequencies. Such phase advances in total over than 90° at very low frequencies, which were not accounted for in the ideal predicted plant, would be the cause of instability occurred for a very high gain in the experimental plant shown in Figure 17. It was also observed in experiments that the use of integrator with the cutoff frequency 10 Hz became unstable with a smaller control gain than that with the cutoff frequency 1 Hz. The reason might be a higher response of the mechanical plant at 10 Hz than 1 Hz. Various methods can be applied to avoid this phase advance effect at very low frequencies, for example, use of a lag compensater, use

of a direct velocity sensor, and use of more ideally performing power amplifiers and integrators. In this report, however, no effort has been made to improve this phase characteristics. It should be emphasised that the purpose of the experimental work was to support the theoretical results rather than to design a practical and perfectly operating active isolation system.

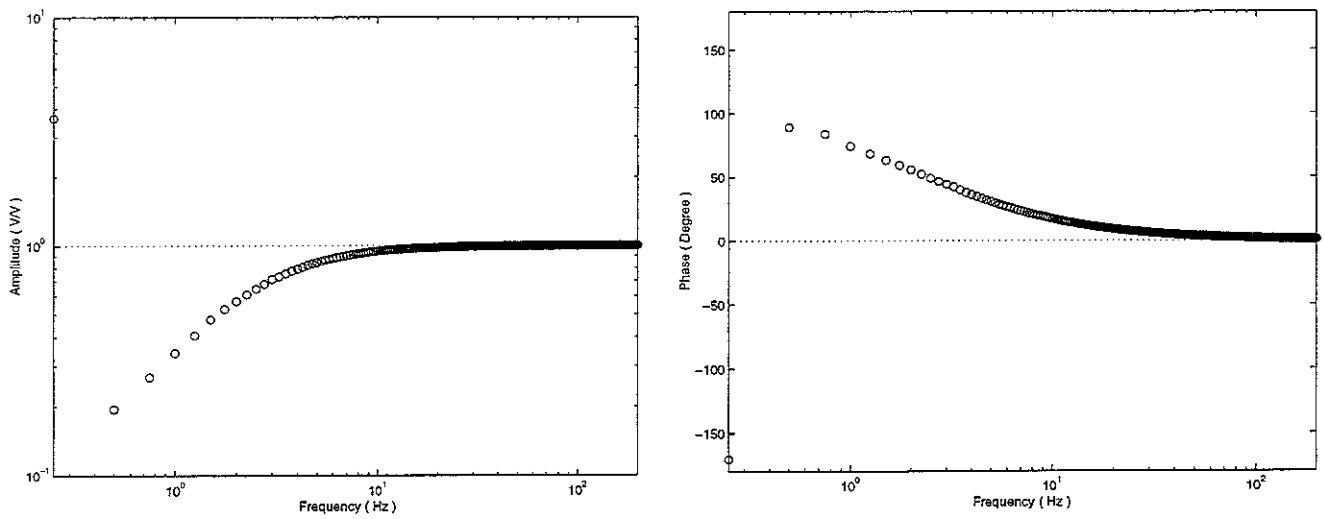

(a) Amplitude (b) Phase

Figure 26. Bode plot of the power amplifier

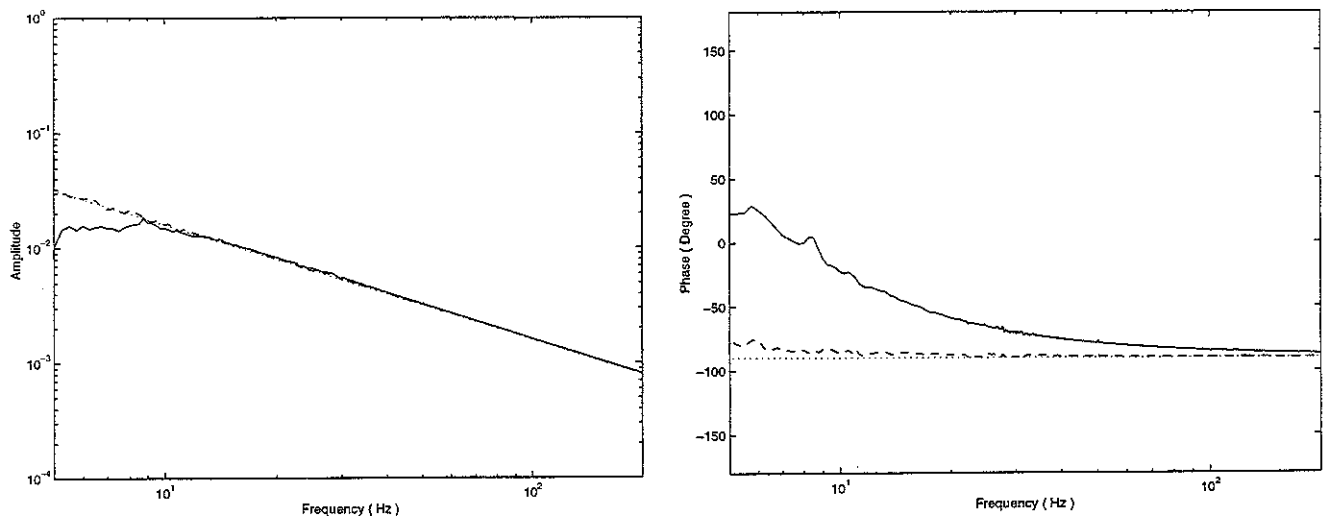

(a) Amplitude (b) Phase

Figure 27. Bode plot of the integrator; with cutoff frequencies 1 Hz(dashed) and 10 Hz(solid). The ideal integrator is shown in dotted line.

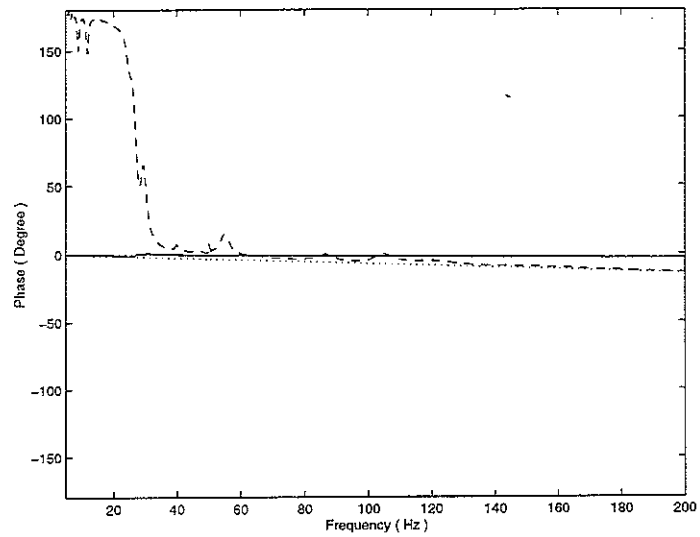

Figure 28. Time delay approximation(dotted line) of the actuator(solid) and the lowpass filter(dashed).

Although an instability was occurred at very low frequencies in the experimental plant, it could also occur at high frequencies due to both electrical and mechanical causes. Use of an electrical lowpass filter for the sensor signal gives a time delay on the control loop, and can cause instability at high frequencies as discussed in Section 3.2. An additional time delay can be caused by the electromagnetic actuator, because there is some time delay between the input voltage and the generated force in the low frequency range[19]. Figure 28 shows the phase responses of a driving point accelerance(dashed line) and the input current response to input voltage of the actuator(solid line). The driving point accelerance can show the time delay due to the lowpass filter, and is compared with a time delay of 0.2 *ms*(dotted line). Also, the current response to input voltage can show the time delay in the electromagnetic actuator, and is compared with a time delay of 0.04 *ms*(dotted line). For the experimental plant considered, the time delay due to the actuator is negligible compared to that due to the lowpass filter. The phase crossover frequency ω_p and the maximum allowable gain value H_{max} due to the total time delay $\tau = 0.24\,ms$ can be calculated from equations (25) and (26) respectively. When the lowest heave mode of mass 6.232 *kg* at 15.8 Hz is considered, they are given by

$$H_{\max} = 40788 \qquad \text{at} \qquad \omega_p = 7.9\,\text{kHz} \tag{60,61}$$

for the gain margin $GM = 1$. In addition to the time delays, the dynamics of the sensors and actuators should be considered in very high frequencies.

The plant can also be potentially unstable at high frequencies due to mechanical causes. It should be emphasised that the mechanical model considered is only valid at low frequencies where the equipment can be modelled as rigid, and the mass effect of the mounts is negligible. At high frequencies, there exist flexible modes within the equipment structure, and so do longitudinal modes within the mounts. The first natural frequency of the thick Al plate for the equipment structure considered can be obtained by [20]

$$f_n = \frac{\lambda t \pi}{2L_x^2}\sqrt{\frac{E}{12\rho(1-\nu^2)}} \approx 1242\,\text{Hz}, \tag{62}$$

where the plate of dimensions (L_x, L_y, t) are L_x=0.3 m, L_y=0.16 m, t=0.02 m, the Young's modulus $E = 71GN/m^2$, the mass density $\rho = 2700kg/m^3$, the Poison's ratio $\nu = 0.33$, and the constant for the first flexible mode for the free-free-free-free plate is given by $\lambda = 2.268$ [20]. The first natural frequency of the longitudinal mode inside a single rubber mount with clamped-clamped boundary conditions can be obtained by [15]

$$f_n = \frac{1}{2h}\sqrt{\frac{E}{\rho}} \approx 500\,\text{Hz}, \tag{63}$$

where the Young's modulus $E = 8\times10^5\,N/m^2$, the mass density $\rho = 909\,kg/m^3$, and the height $h = 0.03m$. Thus above the frequencies in equations (62) and (63), the analytical model described in Section 4.2 is not directly applicable and decentralised velocity feedback control may potentially lead the system unstable.

7. Conclusions

This report has investigated the physical aspects and control mechanisms associated with an active vibration isolation system whose actuators are installed in parallel with each mount between a piece of equipment and a flexible base structure. The control strategy used is *decentralised velocity feedback control*, where each of the four actuators is operated *independently* by feeding back the equipment absolute velocity response at the same location. The special feature of the model is that, although one ends of the actuators are collocated with sensors, the control system is not collocated control because of the supporting force of each actuator acting on the flexible base structure whose dynamics are strongly coupled with the mounted equipment. In particular, isolation of low frequency vibration is considered where the equipment can be modelled as a being rigid and the mounts as lumped parameter springs and dampers. Impedance method is employed for the mechanical analysis of both passive and active vibration isolation systems. A simple single mount system has been useful to investigate mechanical coupling between the mounted equipment and the flexible base as well as control mechanisms. Dynamics and control of a multiple-mount isolation system have been studied by simply extending those for a single mount system. The four-mount active isolation system has been investigated theoretically and experimentally, and important results obtained are as follows.

The system shows collocation control-like behaviours under the assumptions of a rigid equipment and massless mounts; it is unconditionally stable, and perfect vibration isolation is theoretically achievable with an infinite gain. The mechanism involved is that, as the gain increases, the control action uncouples the mounted equipment from the base structure. Equi-decentralised control for a statically balanced symmetric equipment structure is the same as equi-modal control which reduces every vibration mode equivalently. The results from an experimental four-mount active isolation system have been also discussed. The measured system response and closed loop attenuation is very similar to the predicted results, and up to 14 dB reductions in the kinetic energy of the equipment can be achieved in practice. Both simulation and experiment results have shown good agreement with the analytical results. If very high gains were used in the experiments, however, instability was encountered at about 1 Hz due to large phase shift in the electrical equipment used.

References

1. C.E. Crede and J.E. Ruzicka,1996, Shock and Vibration Handbook (C.M. Harris, editor) New York: McGraw-Hill. Ch.30 Theory of vibration isolation
2. L. Meirovitch, 1990, Dynamics and control of structures, John Wiley & Sons, Inc.
3. C.R. Fuller, S.J. Elliott and P.A. Nelson, 1996, Active control of vibration, Academic Press.
4. D. Hrovat and M. Hubbard, 1981, Journal of Dynamic systems, Measurement, and Control, Vol. 103, 228-236, Transactions of the ASME, Optimal Vehicle suspensions minimizing RMS rattlespace, sprung-mass acceleration and jerk.
5. A. Hac, 1986, Journal of Dynamic systems, Measurement, and Control, Vol. 108, 106-110, Transactions of the ASME, Stochastic optimal control of vehicles with elastic body and active suspension
6. M.J. Balas, 1979, Journal of Guidance and Control, Vol. 2, 252-253, Direct velocity feedback control of large space structures
7. S.M. Joshi, 1986, Journal of Guidance and Control, Vol.9, pp.85-91, Robustness properties of collocated controllers for flexible spacecraft
8. D. Karnopp, M.J. Crosby and R.A. Harwood, 1974, Journal of Engineering Industry, pp. 619-626, Vibration control using the semi-active force generators
9. M. Serrand, 1998, MSc Dissertation, University of Southampton, Active isolation of base vibration
10. S. Skogestad and I. Postlethwaite, 1996, Multivariable feedback control; Analysis and design, John Wiley & Sons, Inc.
11. M. Morari and E. Zafiriou, 1989, Robust process control, Prentice-Hall, Inc.
12. S.M. Kim and M.J. Brennan, 1999, Journal of Sound and Vibration, (223), pp.97-113, A compact matrix formulation using the impedance and mobility approach for the analysis of structural-acoustic systems
13. S.M. Kim 1998, PhD Thesis, University of Southampton, Active control of sound in structural-acoustic coupled systems
14. K. Ogata, 1970, Modern control engineering, Prentice-Hall
15. F.S. Tse, I.E. Morse and R.T. Hinkle, 1978, Mechanical Vibrations: Theory and Applications, Allyn and Bacon, Inc.
16. D.J. Mead, 1999, Passive vibration control, John Wiley & Sons Ltd.
17. B. Noble and J.W. Daniel, 1988, Applied Linear Algebra, Prentice-Hall, Inc.
18. F.B. Hilderbrand, 1965, Methods of applied mathematics, Prentice-Hall, Inc. 2nd.
19. M.Z. Ren, K. Seto and F. Doi, 1997, Journal of Sound and Vibration, 205, 57-80, Feedback structural-borne sound control of a flexible plate with an electromagnetic actuator: the phase lag problem
20. G.B. Warbuton, 1951, Proceedings of the Institution of Mechanical Engineers, Vol 168, pp.371-384, The vibration of rectangular plates
21.R.E.D. Bishop and D.C. Johnson, 1960, The mechanics of vibration, Cambridge at the University Press.

Appendix A: Vibration analysis of a rectangular plate

A modal model can be conveniently employed to describe vibration responses in a finite-dimensioned structure, such as a rectangular plate. When the vibration response in a flexible structure is assumed to be described by a summation of N modes, then the vibration velocity at position $\mathbf{r}$ can be written as [13]

$$v(\mathbf{r},\omega) = \sum_{n=1}^{N} \psi_n(\mathbf{r}) a_n(\omega) = \boldsymbol{\psi}^{\mathrm{T}} \mathbf{a} \tag{A1}$$

where the N length column vectors $\boldsymbol{\psi}$ and $\mathbf{a}$ consist of the array of vibration mode shape functions $\psi_n(\mathbf{r})$ and the complex amplitude of the vibration velocity modes $a_n(\omega)$ respectively. The mode shape function $\psi_n(\mathbf{r})$ may be normalised to be the area of the flexible structure $S_f = \int_{S_f} \psi_n^2(\mathbf{r}) dS$ for a convenient calculation of the kinetic energy given in equation (34). When the plate of total mass M_s is subject to a force distribution function $f(\mathbf{r},\omega)$ on its surface, the complex amplitude of the nth mode can be expressed as

$$a_n(\omega) = \frac{1}{M_s} A_n(\omega) \int_{S_f} \psi_n(\mathbf{r}) f(\mathbf{r},\omega) dS \tag{A2}$$

where the structural mass is $M_s = \rho_s h S_f$ where ρ_s is the density of the plate material, h is the thickness of the plate, S_f is the area of flexible structure. The vibration modal resonance term $A_n(\omega)$ is written as:

$$A_n(\omega) = \frac{j\omega}{\omega_n^2 - \omega^2 + j2\zeta_n \omega_n \omega} \tag{A3}$$

where ω_n and ζ_n are the natural frequency and the damping ratio of *n-th* mode, respectively. If the force distribution function is point forces at M number of locations, the modal amplitude vector can be written as [13]

$$\mathbf{a} = \overline{\mathbf{Y}} \mathbf{g} \tag{A4}$$

where the modal mobility matrix $\overline{\mathbf{Y}}$ is given by $\overline{\mathbf{Y}} = \mathbf{A}/M_s$, where $\mathbf{A}$ is a (N×N) diagonal matrix whose (n,n) diagonal term consists of the vibration modal resonance term $A_n(\omega)$ given in equation (A3). For the M number of point forces, the N length generalised force vector $\mathbf{g}$ can be written as:

$$\mathbf{g} = \Psi_M \mathbf{f} \tag{A5}$$

where the M length vector $\mathbf{f}$ denotes the amplitude of M point forces, and the $(N \times M)$ matrix Ψ_M is a transformation matrix which transforms the M length physical force vector $\mathbf{f}$ to the N length generalised force vector $\mathbf{g}$. The transformation matrix consists of a M number of column vectors whose m-th column vector is the mode shape function vector ψ given in equation (A1) at m-th force location. Each element in Ψ_M determines the coupling between modes and force locations, and more specifically its (n, m) element is the amplitude of n-th mode at the m-th force location i.e. $\psi_n(\mathbf{r}_m)$. By substituting equations (A4) and (A5) into (A1), the vibration response at location $\mathbf{r}$ due to M number of forces can be obtained.

The procedure can be easily extended to a multiple-point case where responses at more than one point are of interest. When vibration responses at L number of points are of interest, by extending equation (A1) they can be expressed in vector form as follows:

$$\mathbf{v} = \Psi_L^T \mathbf{a} \tag{A6}$$

where the L length vector $\mathbf{v}$ denotes the vibration velocity responses at L locations, and $\mathbf{a}$ is the modal amplitude vector, and the $(L \times N)$ matrix Ψ_L^T is a transformation matrix which transforms the N length modal amplitude vector $\mathbf{a}$ to the L length physical velocity amplitude vector $\mathbf{v}$. The (m, n) element in Ψ_L^T is the amplitude of n-th mode at the l-th response location i.e. $\psi_n(\mathbf{y}_l)$. Substituting equations (A4) and (A5) into equation (A6) gives

$$\mathbf{v} = \mathbf{Y}\mathbf{f} \tag{A7}$$

where the mobility matrix in physical co-ordinates $\mathbf{Y}_s$ is given by

$$\mathbf{Y} = \Psi_L^T \overline{\mathbf{Y}} \Psi_M \tag{A8}$$

where $\mathbf{Y}$ is of size $(L \times M)$ and whose (l, m) element is the mobility of l-th location due to the m-th point force input. When the response locations of interest are at the force locations as for the base-isolator system considered in this report, the physical mobility matrix becomes a square matrix. Thus, in this case $\mathbf{Y} = \Psi_M^T \overline{\mathbf{Y}} \Psi_M$, where Ψ_M^T is the transpose of Ψ_M. When the number of modes considered are not less than the physical response points considered i.e. $M \leq N$, $\mathbf{Y}$ is generally invertible and thus its impedance representation $\mathbf{Z}$ can be obtained by the inverse of $\mathbf{Y}$. Otherwise, $\mathbf{Z}$ does not exist.

Appendix B. Mode shapes of a rectangular plate

When waveforms in an isotropic thin rectangular plate are assumed to be similar to those of beams, an approximate method presented by Warbuton[20] can be used to describe mode shapes and natural frequencies in the plate. The plate is of dimensions ($L_x \times L_y \times t$), where t is the thickness of the plate and L_x and L_y are lengths in the x and y directions, respectively. Thus, the mode shape function $\psi_n(\mathbf{r})$ at (x, y) in equation (A1) is given by[20]:

$$\psi_n(x,y) = \phi_{nx}(x)\phi_{ny}(y) \tag{B1}$$

where $\phi_{nx}(x)$ and $\phi_{ny}(y)$ are the beam mode shape functions in the x and y directions, and are dependent upon the boundary conditions of the plate. For example, when the plate has a free-free boundary condition in the x direction, then the beam mode for the same boundary condition is used for $\phi_{nx}(x)$. The same applies to $\phi_{ny}(y)$.

For a free-free beam of length L_x, the mode shape functions normalised to be $L_x = \int_0^{L_x} \phi_{nx}^2(x)dx$ are given by [20,21]

$$\phi_{nx}(x) = 1 \qquad \text{for } nx = 0 \tag{B2}$$

$$\phi_{nx}(x) = \sqrt{3}(1 - 2x/L_x) \qquad \text{for } nx = 1 \tag{B3}$$

$$\phi_{nx}(x) = \cosh(k_{nx}x) + \cos(k_{nx}x) - \alpha_{nx}\left(\sinh(k_{nx}x) + \sin(k_{nx}x)\right) \text{ for } nx \geq 2 \tag{B4}$$

where nx denotes the number of nodal points in the x direction, and the coefficient α_{nx} is

$$\alpha_{nx} = \frac{\cosh(k_{nx}L_x) - \cos(k_{nx}L_x)}{\sinh(k_{nx}L_x) - \sin(k_{nx}L_x)} \tag{B5}$$

When $nx = 0$ and $nx = 1$, the mode shape functions are for two rigid body modes of vibration at 0 Hz.

For a clamped-clamped beam of length L_x, the mode shape functions normalised to be $L_x = \int_0^{L_x} \phi_{nx}^2(x)dx$ are given by [20,21]

$$\phi_{nx}(x) = \cosh(k_{nx}x) - \cos(k_{nx}x) - \alpha_{nx}\left(\sinh(k_{nx}x) - \sin(k_{nx}x)\right) \text{ for } nx \geq 2 \tag{B6}$$

where α_{nx} is given in equation (B5) and its explicit values for each boundary condition can be found in [21]. The first beam mode for this boundary condition has two nodal points i.e. $nx = 2$. The vibration mode shape function in the y direction $\phi_{ny}(y)$ can be similarly

normalised to be $L_y = \int_0^{L_y} \phi_{yx}^2(y)dy$, and obtained for the free-free and clamped-clamped boundary conditions. The normalised beam modes in equations (B2-B6) can be substituted to construct the plate modes in equation (B1). From the beam mode shape functions, vibration modes of the plates with free-free-free-free and free-free-clamped-clamped boundary conditions can be described. The resulting plate mode shape function $\psi_n(\mathbf{r})$ satisfies the normalised mode condition $S_f = \int_{S_f} \psi_n^2(\mathbf{r})dS$ that is helpful to calculate the plate kinetic energy given in equation (34). The natural frequencies of the plate for an arbitrary boundary condition has also been discussed in detail by Warbuton[20].